Manipulation of Organolanthanide Coordinative Unsaturation. Synthesis, Structures, Structural Dynamics, Comparative Reactivity, and Comparative Thermochemistry of Dinuclear μ-Hydrides and μ-Alkyls with $[\mu\text{-}R_2Si(Me_4C_5)(C_5H_4)]_2$ Supporting Ligation

David Stern, Michal Sabat, and Tobin J. Marks*

Contribution from the Department of Chemistry, Northwestern University, Evanston, Illinois 60208. *Received May 1, 1990*

Abstract: This contribution describes lutetium and yttrium hydrocarbyl and hydride chemistry based upon the chelating $R_2Si(\eta^5\text{-}C_5H_4)(\eta^5\text{-}Me_4C_5)^{2-}$ ligand (R = Me, Et; abbreviated $R_2SiCpCp''$). The ligand is prepared by reaction of the corresponding $R_2Si(Cp'')Cl$ derivative with NaC_5H_5. Subsequent metalation and reaction with $MCl_3{\cdot}3THF$ (M = Y, Lu) yields $R_2SiCpCp''MCl_2^-Li(OEt_2)_2^+$ complexes, which in turn can be alkylated to yield $R_2SiCpCp''MCHTMS_2$ derivatives (TMS = $SiMe_3$). Pertinent crystallographic data for $Me_2SiCpCp''LuCHTMS_2$ at −120 °C: $P\bar{1}$ (no. 2), $z = 4$, $a = 16.049$ (3) Å, $b = 17.945$ (4) Å, $c = 8.993$ (3) Å, $\alpha = 93.36$ (2)°, $\beta = 90.92$ (2)°, and $\gamma = 82.54$ (2)°; $R(F) = 0.030$ for 6085 independent reflections with $I > 3\sigma(I)$. The structure is of a "bent-sandwich" Cp'_2MX-type ($Cp' = \eta^5\text{-}Me_5C_5$) with relaxed interligand nonbonded interactions vis-ā-vis the Cp'_2M and $Me_2SiCp''_2M$ analogues (Lu–$CHTMS_2$ = 2.365 (7) Å) and having one close Lu···MeSi (Lu–C = 2.820 (8) Å) secondary interaction. These alkyls initiate the polymerization of ethylene and undergo relatively slow hydrogenolysis to yield dihydrides of stoichiometry $(R_2SiCpCp''MH)_2$ via detectable intermediates of stoichiometry $(R_2SiCpCp'')_2M_2(H)(CHTMS_2)$. Pertinent crystallographic data for $(Et_2SiCpCp''LuH)_2$ at −120 °C: $P2_1/n$ (no. 14), $z = 2$, $a = 11.558$ (3) Å, $b = 8.590$ (2) Å, $c = 18.029$ (3) Å, $\beta = 100.10$ (2) Å, $R(F) = 0.022$ for 2656 independent reflections with $I > 3\sigma(I)$. The structure has an idealized C_{2h} $Lu(\mu\text{-}Et_2SiCpCp'')_2(\mu\text{-}H)_2Lu$ geometry with both bridging $Et_2SiCpCp''$ and hydride ligands (Lu–H = 2.16 (4), 2.13 (4) Å). These complexes react slowly (compared to monomeric Cp'_2MH and $Me_2SiCp''_2MH$), reversibly, and regiospecifically with α-olefins to form bridging alkyls of structure $M(\mu\text{-}R_2SiCpCp'')_2(\mu\text{-}H)(\mu\text{-}R')M$, R′ = ethyl, *n*-propyl, *n*-hexyl. Pertinent crystallographic data for $Lu(\mu\text{-}Et_2SiCpCp'')_2(\mu\text{-}H)(\mu\text{-}CH_2CH_3)Lu$ at −120 °C: $P2_1/c$ (no. 14), $z = 6$, $a = 11.679$ (4) Å, $b = 25.755$ (5) Å, $c = 18.074$ (2) Å, $\beta = 99.41$ (2)°; $R(F) = 0.058$ for 4643 independent reflections with $I > 3\sigma(I)$. The $Lu(\mu\text{-}Et_2SiCpCp'')_2(\mu\text{-}H)Lu$ framework is nearly identical to that in the dihydride above. The μ-ethyl fragment is bound very *unsymmetrically* with Lu–C(α) = 2.46 (2) and 2.58 (2) Å, ∠ Lu–C(α)–C(β) = 148 (1)° and 84.7 (5)°. In addition, Lu–C(β) = 2.78 (2) Å suggests a strong secondary bonding interaction. Hydrogenolysis of the μ-alkyl linkages is considerably slower than for terminal alkyl bonds in $Cp'_2M(alkyl)$ and $Me_2SiCp''_2M(alkyl)$ complexes. NMR studies of the μ-alkyls reveal rapid rotation of the μ-alkyl ligands about the μ-H-μ-C(α) vectors down to −85 °C and rapid inversion at C(α) occurring with $\Delta G^{\ddagger} = 12.5\text{–}13.5$ kcal/mol ($T_c = +11 - +39$ °C). Kinetic (rate law: $v = k$[dihydride][olefin]) and equilibration measurements reveal that the hydride addition process to 1-hexene $(Et_2SiCpCp''LuH)_2$ + 1-hexene ⇄ $Lu(\mu Et_2SiCpCp)_2(\mu\text{-}H)(\mu\text{-}n\text{-hexyl})Lu$ is described by $\Delta H = -10.7$ (6) kcal/mol, $\Delta S = -25$ (2) eu, $\Delta H^{\ddagger} = 12.0$ (4) kcal/mol, and $\Delta S^{\ddagger} = -38.6$ (7) eu. These results indicate that, in comparison to terminal bonding modes with similar metal ancillary ligation, lanthanide μ-H ligands are kinetically *deactivated* with respect to olefin insertion (a rate depression of $\sim 10^8\text{–}10^{10}$), and μ-alkyl ligands are kinetically *deactivated* with respect to hydrogenolysis (a rate depression of $\sim 10^8\text{–}10^9$). Moreover, relative to a bridging hydride ligand, lanthanide μ-alkyl coordination is found to be no more and probably less thermodynamically stable than terminal alkyl coordination.

The stoichiometric and catalytic properties of organo-f-element hydrocarbyls and hydrides[1,2] are profoundly influenced by the nature of π ancillary ligands. Structurally, the ligational transposition $Cp'_2MX_n \rightarrow Me_2SiCp''_2MX_n$ ($Cp' = \eta^5\text{-}Me_5C_5$; $Cp'' = \eta^5\text{-}Me_4C_5$; X = σ-bonded ligand)[3-5] results in a considerable opening of the metal coordination sphere in the vicinity of the σ ligand equatorial girdle[3,4]/frontier orbitals.[6] For organolanthanides A and B, this modification effects large increases (ca.

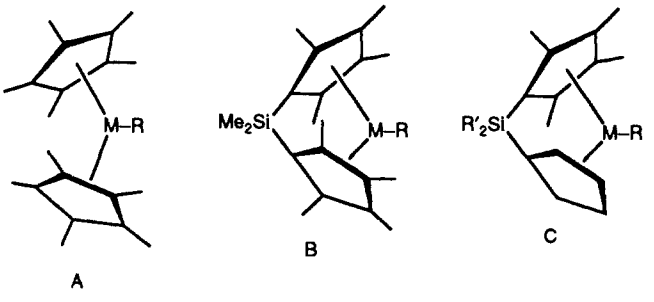

10–100-fold) in rates of olefin insertion into M–R bonds, where R = H,[3] alkyl,[3] and alkylamide.[7] This same modification in

(1) (a) *Fundamental and Technological Aspects of Organo-f-Element Chemistry*; Marks, T. J., Fragalā, I., Eds.; D. Reidel: Dordrecht, Holland, 1985. (b) Marks, T. J.; Ernst, R. D. In *Comprehensive Organometallic Chemistry*; Wilkinson, G., Stone, F. G. A., Abel, E. W., Eds.; Pergamon Press: Oxford, 1982; Chapter 21.

(2) (a) Schumann, H.; Albrecht, I.; Gallagher, M.; Hahn, E.; Janiak, C.; Kolax, C.; Loebel, J.; Nickel, S.; Palamedis, E. *Polyhedron* **1988**, *7*, 2307–2315. (b) Evans, W. J. *Polyhedron* **1987**, *6*, 803–835. (c) Marks, T. J.; Streitwieser, A., Jr. In *The Chemistry of the Actinide Elements*, 2nd ed.; Katz, J. J., Seaborg, G. T., Morss, L. R., Eds.; Chapman and Hall: London, 1986; Chapter 22. (d) Marks, T. J. *Ibid.* Chapter 23. (e) Schumann, H. in ref 1a, Chapter 1. (f) Evans, W. J. *Adv. Organomet. Chem.* **1985**, *24*, 131–177. (g) Watson, P. L.; Parshall, G. W. *Acc. Chem. Res.* **1985**, *18*, 51–56.

(3) (a) Jeske, C.; Schock, L. E.; Mauermann, H.; Swepston, P. N.; Schumann, H.; Marks, T. J. *J. Am. Chem. Soc.* **1985**, *107*, 8103–8110. (b) Jeske, G.; Lauke, H.; Mauermann, H.; Schumann, H.; Marks, T. J. *J. Am. Chem. Soc.* **1985**, *107*, 8111–8118.

(4) (a) Fendrick, C. M.; Schertz, L. D.; Schertz, L. D.; Day, V. W.; Marks, T. J. *Organometallics* **1988**, *7*, 1828–1838. (b) Fendrick, C. M.; Mintz, E. A.; Schertz, L. D.; Marks, T. J.; Day, V. W. *Organometallics* **1984**, *3*, 819–821.

(5) For related studies using chelating C_5Me_4 ligands in d block chemistry, see: (a) Jützi, P.; Dickbreder, R. *Chem. Ber.* **1986**, *119*, 1750–1754. (b) Scholz, H. J.; Werner, H. *J. Organometal. Chem.* **1986**, *303*, C8–C12. (c) Wochner, F.; Zsolnai, L.; Huttner, G.; Brintzinger, H. H. *J. Organomet. Chem.* **1985**, *288*, 69–77.

(6) (a) Bursten, B. E.; Strittmatter, R. J. *Angew. Chem., Int. Ed. Engl.*, in press. (b) Tatsumi, K.; Nakamura, A. *J. Am. Chem. Soc.* **1987**, *109*, 3195–3206. (c) Tatsumi, K.; Nakamura, A.; Hoffman, P.; Hoffman, R.; Moloy, K. G.; Marks, T. J. *J. Am. Chem. Soc.* **1986**, *108*, 4467–4476. (d) Bursten, B. E.; Fang, A. *Inorg. Chim. Acta* **1985**, *110*, 153–160, and references therein.

0002-7863/90/1512-9558$02.50/0

Th(IV) chemistry effects a 10^3-fold increase in catalytic activity for 1-hexene hydrogenation.[4] In an effort to further open the metal coordination sphere while still preserving the frontier orbitals[6] and other advantages of Cp'_2M ancillary ligation,[1-5] we have explored the properties of lanthanide complexes based upon $R_2SiCpCp''$ supporting coordination C ($Cp = \eta^5$-C_5H_4).[8,9] We report here a full synthetic, structural, and kinetic/mechanistic discussion of our findings for M = Lu and Y. It will be seen that the chemistry is rather different than that of systems A and B, with an unprecedented $2R_2SiCpCp''Ln- \rightarrow -Ln(\mu\text{-}R_2SiCpCp'')_2Ln-$ rearrangement dominating the hydride chemistry and offering a route to an unusual series of binuclear μ-H and μ-alkyl complexes. Historically, transition-metal μ-alkyl moieties have often been associated with special reactivity properties,[10] and the present study provides the first opportunity to *quantitatively* assess these reactivity characteristics as well as the kinetics and thermodynamics of μ-H $\rightleftharpoons$ μ-alkyl interconversions vis-à-vis those of the terminal (unbridged) analogues. The differences are found to be very substantial.

Experimental Section

Materials and Methods. All manipulations were performed with the rigorous exclusion of oxygen and moisture in flamed, Schlenk-type glassware on a dual manifold Schlenk line or interfaced to a high vacuum (10^{-5} Torr) line or in a nitrogen-filled Vacuum Atmospheres glovebox with a high capacity recirculator. Argon (Matheson, prepurified), hydrogen (Linde), deuterium (99.5%, Matheson), ethylene (Matheson, CP), *trans-1,2-*d_2 and *1,2-*^{13}C labeled ethylene (98 and 99 atom % d_2 and $^{13}C_2$, respectively, Cambridge Isotopes), propylene (Matheson, CP), and *cis*-2-butene (Matheson, CP) were purified by passage through a supported MnO oxygen removal column and a Davison 4Å molecular sieve column.[11] Aliphatic hydrocarbon solvents were pretreated with concentrated H_2SO_4 and $KMnO_4$ solution.[12] All reaction solvents were distilled from Na/K/benzophenone under nitrogen and were stored in vacuo over Na/K alloy in bulbs on the vacuum line. Deuterated solvents were obtained from Cambridge Isotope Laboratories (all ≥99 atom % D) and were degassed and dried over Na/K alloy (benzene-d_6, toluene-d_8, tetrahydrofuran-d_8 (THF-d_8), and cyclohexane-d_{12}) or P_2O_5 ($CDCl_3$) before use. Anhydrous metal trichlorides were prepared from the corresponding oxides.[13] They were converted to the corresponding THF complexes by Soxhlet extraction with THF.[3] The ligand precursors 2,3,4,5-tetramethylcyclopent-2-enone and 1,2,3,4-tetramethylcyclopentadienone were prepared by published procedures[4a] and were distilled immediately prior to use. Bis(trimethylsilyl)methyllithium ($LiCHTMS_2$) was prepared by the literature method.[14] Dimethyl- and diethyldichlorosilane (Petrarch) were dried over P_2O_5 and distilled prior to use. Sodium cyclopentadienide was prepared by a literature procedure,[15] and the solid reagent was dried in vacuo overnight. Solutions of methyllithium and *n*-butyllithium (Aldrich) were used as received.

Physical and Analytical Measurements. ^1H NMR spectra were recorded on either a Varian EM-390 (CW, 90 MHz), a JEOL FX-270 (FT, 270 MHz) or a Varian XL-400 (FT, 400 MHz) spectrometer. ^{13}C NMR spectra were recorded at 67.8 MHz on a JEOL FX-270 or at 100 MHz on a Varian XL-400. Chemical shifts were referenced to internal solvent resonances and are reported relative to TMS. Spin-lattice relaxation time measurements were carried out on the Varian XL-400 by using the inversion-recovery subroutine DOTI. NOE difference spectra, spin simulation analyses, and double irradiation experiments were also carried out with the XL-400. IR spectra were recorded on a Perkin-Elmer 599B spectrophotometer. Samples were examined neat, as Nujol mulls, or as KBr pellets sandwiched between KBr plates in an O-ring sealed, air-tight holder. As a routine precaution, one compound from each class was examined in both KBr and Nujol to ensure that no reaction was occurring with the dispersing agent. Elemental analyses were performed by Dornis and Kolbe Mikroanalytisches Laboratorium, Mülheim, West Germany, or by Oneida Research Services, Inc., Whitesboro, NY.

$Me_2Si(Cp''H)Cl$. Freshly distilled tetramethylcyclopentadiene (Cp''H, 11 g, 0.090 mol) and pentane (150 mL) were syringed, under argon flush, into a three-necked, 500-mL flask equipped with dropping funnel, magnetic stirring bar, and gas inlet adapter. *n*-Butyllithium (56 mL of a 1.6 M solution in hexane, 0.090 mol) was syringed into the stirred solution, and a milky white suspension of LiCp'' was evident within minutes. After stirring the reaction mixture at room temperature for 12 h, THF (150 mL) was added, and the solid mass of LiCp'' was broken up with the aid of an external magnet. The resulting solution was next cooled to 0 °C, and a solution of Me_2SiCl_2 (11.6 g, 0.090 mol) in THF (30 mL) was added dropwise with stirring over a 1 h period. The reaction mixture was allowed to stir at room temperature for another 12 h. The suspension was then filtered through a Celite-packed frit, and the solvent was removed under reduced pressure. Fractional distillation at 56–59 °C/0.1 Torr yielded 13.5 g (70%) of a pale yellow oil: ^1H NMR (90 MHz, benzene-d_6) δ 2.89 (s, 1 H), 1.90 (s, 6 H), 1.71 (s, 6 H), 0.14 (s, 6 H); IR (neat, cm^{-1}) 2975 vs, 2920 vs, 2867 vs, 1635 m, 1550 w, 1447 s, 1410 m, 1390 m, 1307 w, 1258 s, 1218 m, 1118 m, 1052 m, 1025 m, 991 s, 958 m, 843 s, 817 s, 790 s, 740 w, 693 w, 657 s, 510 s, 463 s.

$Me_2SiCpCp''Li_2{\cdot}2THF$. A 500-mL Schlenk flask with a 50-mL addition funnel was charged with 10.6 g (49.0 mmol) of freshly distilled $Me_2Si(Cp''H)Cl$. THF (100 mL) was added to the reaction flask, and the resulting solution was cooled to 0 °C. A solution of NaCp in THF (35 mL of a 1.4 M solution, 49 mmol) was cannula-transferred to the additional funnel and was added dropwise to the stirring reaction mixture over a period of 45 min. The reaction was then allowed to proceed for 10 h at 0 °C, during which time a white precipitate (NaCl) formed. Stirring was continued for another 2 h at room temperature to ensure complete reaction. This mixture was next recooled to 0 °C, and a solution of methyllithium in diethyl ether (70 mL of a 1.4 M solution; 98 mmol) was added dropwise. Methane evolution was apparent. The reaction was stirred for 6 h at 0 °C and then 12 h at room temperature. The solvent volume was next reduced to ca. 20 mL, diethyl ether (150 mL) was added, and the resulting slurry was filtered. The white solids which collected were washed with diethyl ether (3 × 50 mL) and dried in vacuo: yield 18.2 g (81%); ^1H NMR (THF-d_8) δ 5.88 ("t", J_{HH} = 2.6 Hz, 2 H), 5.73 ("t", J_{HH} = 2.5 Hz, 2 H), 2.04 (s, 6 H), 1.86 (s, 6 H), 0.35 (s, 6 H); IR (Nujol, cm^{-1}) 2890 vs, 1460 s, 1380 s, 1318 m, 1265 s, 1248 m, 1102 br s, 1040 br s, 867 w, 810 vs, 738 s, 639 m, 611 m, 460 m.

$Et_2Si(Cp''H)Cl$. A 2-L Schlenk flask equipped with a 250-mL dropping funnel was charged with freshly distilled Cp''H (18.6 g, 0.152 mol) and THF (600 mL). Next, a solution of *n*-butyllithium (1.6 M solution in hexane, 0.152 mol) was added with stirring, and the mixture was stirred for 10 h, during which time LiCp'' precipitation and butane evolution were apparent. The reaction mixture was then cooled to 0 °C, and a solution of Et_2SiCl_2 (23.0 mL, 0.152 mol) in THF (50 mL) was added dropwise. After Et_2SiCl_2 addition was complete, stirring at 0 °C was continued for an additional 2 h and then for 10 h at room temperature. The THF was next removed under reduced pressure, pentane (200 mL) was added, and the solution filtered. The solvent was removed from the filtrate under reduced pressure, and the liquid product was purified by fractional distillation through a Vigreaux column. The yellow oil boiling at 67–74 °C/20 μm was collected: yield 23.9 g (88%); ^1H NMR (benzene-d_6) δ 3.03 (m, 1 H), 1.96 (s, 6 H), 1.73 (s, 6 H), 0.95 (t, 6 H), 0.56 (q, 4 H); IR (neat, cm^{-1}) 2960 vs, 2880 s, 1630 m, 1460 s, 1410 m, 1380 m, 1230 m, 1110 s, 1010 s, 950 m, 765 m, 720 s, 610 s.

(7) (a) Gagné, M. R.; Marks, T. J. *J. Am. Chem. Soc.* **1989**, *111*, 4108–4109. (b) Gagné, M. R.; Marks, T. J. *Abstracts of Papers*, 197th National Meeting of the American Chemical Society, Dallas, TX, April 9–14, 1989; American Chemical Society: Washington, DC, 1989; INOR 32. (c) Gagné, M. R.; Marks, T. J., manuscript in preparation.

(8) Preliminary communication: Stern, D.; Sabat, M.; Marks, T. J. *Abstracts of Papers*, 196th National Meeting of the American Chemical Society, Los Angeles, CA, September 25–30, 1988; American Chemical Society: Washington, DC, 1988; INOR.

(9) For the use of chelating $X(C_5H_4)_2$ ligands in organo-f-element chemistry, see: (a) Qian, C.; Ye, C.; Li, Y. *J. Organomet. Chem.* **1986**, *302*, 171–179. (b) Qian, C.; Ye, C.; Lu, H.; Li, Y.; Huang, Y. *J. Organomet. Chem.* **1984**, *263*, 333–343, and references therein. (c) John, J. N.; Tsutsui, M. *Inorg. Chem.* **1981**, *20*, 1602–1604. (d) Marks, T. J. *Adv. Chem. Ser.* **1976**, *150*, 232–255. (e) Secaur, C. A.; Day, V. W.; Ernst, R. D.; Kennelly, W. J.; Marks, T. J. *J. Am. Chem. Soc.* **1976**, *98*, 3713–3715.

(10) (a) Gavens, P. D.; Bottrill, M.; Kelland, J. W.; McMesking, J. in ref 1b, Chapter 22.5. (b) Sinn, H.; Kaminsky, W. *Adv. Organomet. Chem.* **1980**, *18*, 99–149. (c) Boor, J., Jr. *Ziegler-Natta Catalysts and Polymerizations*; Academic Press: New York, 1979.

(11) (a) This material is reported to reduce the O_2 content of flowing inert gas streams to the ppb range.[11b-d] (b) Moeseler, R.; Horvath, B.; Lindenau, D.; Horvath, E. G.; Krauss, H. L. *Z. Naturforsch., B* **1976**, *31B*, 892–893. (c) McIlwrick, C. R.; Phillips, C. S. G. *J. Chem. Phys. E* **1973**, *6*, 1208–1210. (d) He, M.-Y.; Xiong, G.; Toscano, P. J.; Burwell, R. L., Jr.; Marks, T. J. *J. Am. Chem. Soc.* **1985**, *107*, 641–652.

(12) Perrin, D. D.; Armarego, W. L. F.; Perrin, D. R. *Purification of Laboratory Chemicals*, 2nd ed.; Pergamon Press: Oxford, 1980.

(13) Brauer, G. *Handbuch der Praparativen Anorganischen Chemie*; F. Enke Verlag: Stuttgart, 1962; Vol. 2, p 1002.

(14) Cowley, A. H.; Kemp, R. A. *Synth. React. Inorg. Met.-Org. Chem.* **1981**, *11*, 591–595.

(15) *Organometallic Syntheses*; Eisch, J. J., King, R. B., Eds.; Academic Press: New York, 1965; p 64.

$Et_2Si(CpH)(Cp''H)$. A 1-L Schlenk flask was charged with $Et_2Si(Cp''H)Cl$ (32.1 g, 0.132 mol) and THF (400 mL). The flask was cooled to −78 °C, and a solution of NaCp in THF (94 mL of a 1.4 M solution, 0.132 mol) was added, with stirring, under an argon flush. The reaction mixture was slowly warmed to 0 °C, stirred for 2 h, and then stirred for 18 h at room temperature. The solvent was next removed under reduced pressure, pentane (150 mL) was added, and the solution was filtered through a Celite 545-packed frit. Attempts to solidify or crystallize the product were unsuccessful, so the solvent was removed in vacuo, and the resulting viscous yellow oil was used without further purification: yield 29.3 g (82%); ^1H NMR (benzene-d_6) δ 6.8–6.4 (m, 4 H), 3.1–2.8 (m, 2 H), 2.0–1.7 (12 H), 1.1–0.4 (m, 10 H); IR (neat, cm^{-1}) 2960 vs, 2880 vs, 1630 w, 1450 s, 1410 m, 1380 m, 1258 m, 1215 m, 1110 s, 1053 s, 1008 vs, 948 s, 792 m, 710 vs.

$Et_2SiCpCp''Li_2{\cdot}2THF$. A 1-L Schlenk flask was charged with $Et_2Si(CpH)(Cp''H)$ (41.1 g, 0.151 mol). THF (200 mL) was added to this oil, and the resulting solution was cooled to −78 °C. *n*-Butyllithium (188 mL of a 1.6 M solution in hexane, 0.30 mol) was then added with stirring, and the reaction mixture was allowed to warm to room temperature over a period of 4 h. A white precipitate became apparent by −10 °C. The reaction mixture was then stirred at room temperature for another 18 h. The solvent volume was next reduced in vacuo to ca. 70 mL, and the colorless microcrystalline product was collected on a frit and washed with pentane (3 × 30 mL): yield 42 g (65%); ^1H NMR (THF-d_8) δ 5.88 ("t", J_{HH} = 2.7 Hz, 2 H), 5.75 ("t", J_{HH} = 2.4 Hz), 2.04 (s, 6 H), 1.87 (s, 6 H), 1.02–0.93 (m, 10 H); IR (Nujol, cm^{-1}) 2980 vs, 1590 w, 1465 vs, 1380 vs, 1351 w, 1318 m, 1260 w, 1222 w, 1178 m, 1040 vs, 1010 m, 918 m, 898 m, 821 m, 742 s, 710 s, 680 m, 668 m, 628 m, 483 m.

$Me_2SiCpCp''LuCl_2^-{\cdot}Li(ether)_2^+$ (1). A 100-mL flask was charged with $LuCl_3{\cdot}3THF$ (2.23 g, 4.47 mmol) and $Me_2SiCpCp''Li_2{\cdot}2THF$ (2.05 g, 4.47 mmol). THF (75 mL) was condensed into the flask in vacuo at −78 °C. After backfilling with argon, the reaction mixture was heated to reflux with stirring for 18 h. During this time, the milky white suspension dissolved to yield a golden-colored solution. The solvent was then removed in vacuo, and diethyl ether (40 mL) was condensed onto the solids. After stirring this mixture for 10 min, the ether was removed in vacuo taking care not to warm the flask above room temperature. This ether exchange procedure was repeated twice, the final ether solution was filtered, and the filtrate was slowly cooled to −78 °C. The resulting colorless crystals were isolated by cold filtration and were dried in vacuo to yield 1.88 g (65%) of $Me_2SiCpCp''LuCl_2^-Li(ether)_2^+$. An additional 0.32 g (11%) of product can be recovered from the mother liquor (total yield: 76%). This compound is not soluble enough in benzene or toluene to obtain an ^1H-NMR spectrum. After heating at 60 °C in $CDCl_3$, this compound loses LiCl and ether. The ^1H-NMR spectrum suggests a species such as $(Me_2SiCpCp''LuCl)_2$:[16] ^1H NMR (decomposition product in $CDCl_3$) δ 6.71 ("t", 2 H), 5.78 ("t", 2 H), 2.07 (s, 6 H), 1.95 (s, 6 H), 0.85 (s, 6 H); IR (KBr, cm^{-1}) 2900 vs, 1435 m, 1375 s, 1310 m, 1240 s, 1150 s, 1050 s, 890 m, 800 s, 660 m. Anal. Calcd for $C_{24}H_{42}SiCl_2LiO_2Lu$: C, 44.80; H, 6.57. Found: C, 44.70; H, 6.44.

$Et_2SiCpCp''LuCl_2^-Li^+(ether)_2$ (2). The procedure described above for the synthesis of $Me_2SiCpCp''LuCl_2^-Li(ether)_2^+$ (**1**) was followed with 3.44 g (6.91 mmol) of $LuCl_3{\cdot}3THF$ and 2.94 g (6.85 mmol) of $Et_2SiCpCp''Li_2{\cdot}2THF$ in 70 mL of THF. Recrystallization from 30 mL of diethyl ether at −78 °C yielded 2.94 g (68%) of colorless, crystalline product. An additional 0.51 g (12%) of product can be recovered from the mother liquor (total yield 80%): ^1H NMR (benzene-d_6) δ 6.87 ("t", 2 H), 5.73 ("t", 2 H), 3.25 (q, 8 H), 2.11 (s, 6 H), 1.92 (s, 6 H), 1.4–1.25 (m, 10 H), 1.11 (t, 12 H); IR (Nujol, cm^{-1}) 2920 vs, 2740 w, 1455 vs, 1378 s, 1321 m, 1230 w, 1172 m, 1123 s, 1046 s, 1008 m, 978 w, 843 m, 818 w, 778 s, 722 s, 683 s, 671 w, 638 m, 494 s, 420 m. Anal. Calcd for $C_{26}H_{46}SiCl_2LiO_2Lu$: C, 46.50; H, 6.90. Found: C, 46.44; H, 6.95.

$Et_2SiCpCp''YCl_2^-Li(ether)_2^+$ (3). The aforementioned procedure for the synthesis of $Me_2SiCpCp''LuCl_2^-Li(ether)^+$ (**1**) was carried out with 2.80 g (6.80 mmol) of $YCl_3{\cdot}3THF$ and 2.92 g (6.80 mmol) of $Et_2SiCpCp''Li_2{\cdot}2THF$ in 70 mL of THF. Workup as described above yielded 2.58 g (69%) of $Et_2SiCpCp''YCl_2^-Li(ether)^+$ as colorless microcrystals: ^1H NMR (benzene-d_6) δ 6.84 ("t", J_{HH} = 2.1 Hz, 2 H), 5.78 ("t", J_{HH} = 2.2 Hz, 2 H), 3.26 (q, $^3J_{HH}$ = 6.9 Hz, 8 H), 2.06 (s, 6 H), 1.91 (s, 6 H), 1.38–1.24 (m, 10 H), 1.11 (t, $^3J_{HH}$ = 6.9 Hz, 12 H); IR (Nujol, cm^{-1}) 2920 vs, 2730 m, 1613 w, 1460 s, 1380 s, 1320 m, 1230 w, 1170 m, 1122 s, 1062 w, 1044 s, 1008 m, 972 w, 900 w, 845 s, 778 s, 752 m, 722 s, 682 s, 638 m, 497 s, 428 m. Anal. Calcd for $C_{26}H_{46}SiCl_2LiO_2Y$: C, 53.34; H, 7.92. Found: C, 53.27; H, 7.90.

$Me_2SiCpCp''LuCH(TMS)_2$ (4). A 70-mL flask was charged with 3.02 g (4.70 mmol) of $Me_2SiCpCp''LuCl_2^-Li(ether)_2^+$ (**1**) and 0.78 g (4.70 mmol) of $LiCH(TMS)_2$. Toluene (40 mL) was next condensed into the flask in vacuo at −78 °C. Argon was then admitted to the flask and the suspension was allowed to warm to room temperature and was stirred for 12 h. The toluene was removed in vacuo, and the off-white residue was extracted with 50 mL of pentane. The resulting mixture was filtered, the volume of filtrate was reduced to 25 mL, and the filtrate was slowly cooled to −78 °C. Large, colorless crystals were isolated by decantation and subsequent vacuum drying: yield 2.44 g (90%); ^1H NMR (benzene-d_6) δ 6.66 ("t", J_{HH} = 2.5 Hz, 2 H), 5.52 ("t", J_{HH} = 2.5 Hz, 2 H), 1.81 (s, 6 H) 1.80 (s, 6 H), 0.75 (s, 6 H), 0.09 (s, 18 H), −0.50 (s, 1 H); ^{13}C NMR (benzene-d_6) δ 126.0 (s), 120.8 (s), 119.4 (s), 118.0 (d, $^1J_{CH}$ = 168 Hz), 113.0 (d, $^1J_{CH}$ = 165 Hz), 108.2 (s), 29.1 (d, $^1J_{CH}$ = 93 Hz), 13.8 (q, $^1J_{CH}$ = 126 Hz), 11.9 (q, $^1J_{CH}$ = 126 Hz), 3.8 (q, $^1J_{CH}$ = 117 Hz), 0.3 (q, $^1J_{CH}$ = 120 Hz); IR (KBr, cm^{-1}) 2940 s, 2900 s, 1440 m, 1380 m, 1310 m, 1250 s, 1060 m, 1040 s, 990 m, 830 s, br, 770 s, 670 s, 570 sh, 380 m. Anal. Calcd for $C_{23}H_{41}Si_3Lu$: C, 47.89; H, 7.16; Si, 14.61. Found: C, 47.95; H, 7.22; Si, 14.61.

$Et_2SiCpCp''LuCH(TMS)_2$ (5). The preceding synthesis for **4** was carried out with 2.37 g (3.53 mmol) of $Et_2SiCpCp''LuCl_2^-Li(ether)^+$ (**2**) and 0.587 g (3.53 mmol) of $LiCH(TMS)_2$ in 60 mL of toluene: yield 1.52 g (71%) of $Et_2SiCpCp''LuCH(TMS)_2$ as colorless crystals; ^1H NMR (benzene-d_6) δ 6.66 ("t", J_{HH} = 2.4 Hz, 2 H), 5.53 ("t", J_{HH} = 2.4 Hz, 2 H), 1.82 (s, 6 H), 1.81 (s, 6 H) 1.38–1.24 (m, 10 H), 0.09 (s, 18 H), −0.52 (s, 1 H); IR (Nujol, cm^{-1}) 2910 vs, 1454 vs, 1378 vs, 1321 m, 1239 w, 1230 w, 1162 m, 1154 m, 1124 s, 1067 m, 1045 s, 1008 s, 976 w, 899 w, 860 w, 842 s, 818 m, 779 s, 758 m, 721 s, 683 s, 672 m, 636 m, 496 m, 421 w. Anal. Calcd for $C_{25}H_{45}LuSi_3$: C, 49.64; H, 7.50. Found: C, 49.60; H, 7.52.

$Et_2SiCpCp''YCH(TMS)_2$ (6). The procedure described above for **4** was carried out with 1.72 g (2.94 mmol) of $Et_2SiCpCp''YCl_2^-Li(ether)^+$ (**3**) and 0.490 g (2.94 mmol) of $LiCH(TMS)_2$ in 50 mL of toluene. Following recrystallization from pentane at −78 °C, 1.02 g (67%) of colorless crystalline $Et_2SiCpCp''YCH(TMS)_2$ was isolated by cold filtration: ^1H NMR (benzene-d_6) δ 6.69 ("t", J_{HH} = 2.4 Hz, 2 H), 5.58 ("t", J_{HH} = 2.4 Hz, 2 H), 1.82 (s, 6 H), 1.81 (s, 6 H), 1.35–1.23 (m, 10 H), 0.08 (s, 18 H), −0.59 (d, J_{YH} = 2.5 Hz, 1 H); ^{13}C NMR (toluene-d_8) δ 126.3 (s), 122.8 (s), 118.2 (d, $^1J_{CH}$ = 167 Hz), 116.1 (s), 115.0 (d, $^1J_{CH}$ = 165 Hz), 106.5 (s), 29.3 (dd, $^1J_{CH}$ = 93.4 Hz, J_{YC} = 31 Hz), 13.6 (q, $^1J_{CH}$ = 126 Hz), 11.9 (q, $^1J_{CH}$ = 125 Hz), 7.4 (q, $^1J_{CH}$ = 126 Hz), 4.9 (t, $^1J_{CH}$ = 119 Hz), 3.7 (q, $^1J_{CH}$ = 115 Hz); IR (Nujol, cm^{-1}) 2930 vs, 2740 w, 1460 vs, 1378 s, 1310 w, 1267 m, 1241 m, 1168 w, 1040 s, 1012 w, 861 s, 827 s, 810 m, 788 s, 752 m, 718 m, 683 m, 631 w, 572 w, 491 w, 422 w. Anal. Calcd for $C_{25}H_{45}Si_3Y$: C, 57.88; H, 8.74. Found: C, 57.85; H, 8.75.

$(Me_2SiCpCp''LuH)_2$ (12). A 50-mL flask was charged with 1.15 g (2.00 mmol) of **4**. Pentane (20 mL) was condensed into the flask in vacuo at −78 °C, and the vessel was backfilled with 1 atm of H_2. The solution was then stirred for 4 days at room temperature, while the product precipitated from solution. The resulting colorless microcrystals were collected by filtration, washed with pentane (2 × 5 mL), and dried in vacuo: yield 0.68 g (82%); ^1H NMR (benzene-d_6) δ 6.32 ("t", J_{HH} = 2.5 Hz, 2 H), 6.17 ("t", J_{HH} = 2.5 Hz, 2 H), 5.92 (s, 1 H), 2.07 (s, 6 H), 2.05 (s, 6 H), 0.61 (s, 6 H); IR (KBr, cm^{-1}) 2900 s, 1440 m, 1410 m, 1380 m, 1360 m, 1320 s, 1220 br s, 1130 m, 1060 m, 1040 s, 1015 m, 910 s, 810 vs, 770 vs, 645 s, 455 m, 415 m, 370 m. Anal. Calcd for $C_{32}H_{46}Si_2Lu_2$: C, 45.93; H, 5.54; Lu, 41.82. Found: C, 45.96; H, 5.58; Lu, 41.64.

$(Et_2SiCpCp''LuH)_2$ (13). A solution of 1.20 g (1.98 mmol) of **5** in 30 mL of pentane was stirred under 1 atm of H_2 at room temperature for 4 days. The precipitated product was collected by filtration, washed with pentane (2 × 5 mL), and dried in vacuo to yield 0.77 g (82%) of $(Et_2SiCpCp''LuH)_2$ as a colorless, microcrystalline solid: ^1H NMR (toluene-d_8) δ 6.22 ("t", J_{HH} = 2.5 Hz, 2 H), 6.13 ("t", J_{HH} = 2.6 Hz, 2 H), 5.87 (s, 1 H), 2.063 (s, 6 H), 2.058 (s, 6 H), 1.29–1.06 (m, 4 H), 1.02 (t, $^3J_{HH}$ = 7.5 Hz, 6 H); IR (Nujol, cm^{-1}) 2920 vs, 2860 vs, 1460 vs, 1377 s, 1321 m, 1230 br s, 1178 w, 1042 m, 1012 m, 969 w, 926 m, 793 s, 750 w, 726 m, 708 m, 650 m, 620 m, 503 m, 438 m. Anal. Calcd for $C_{36}H_{54}Si_2Lu_2$: C, 48.42; H, 6.10. Found: C, 48.40; H, 6.13.

$(Et_2SiCpCp''LuD)_2$ (13d) was synthesized in a similar manner to **13** under 1 atm of D_2. The IR spectrum in Nujol is nearly identical with that of the hydride except for the absence of peaks at 1230, 926, 650 and the presence of new peaks at 882 s, 661 m, and 480 w cm^{-1}.

$(Et_2SiCpCp''YH)_2$ (14). The procedure described above for the synthesis of **13** was repeated with 0.67 g (1.16 mmol) of $Et_2SiCpCp''YCH(TMS)_2$: yield 0.368 g (88%) of colorless, microcyrstalline $(Et_2SiCpCp''YH)_2$; ^1H NMR (benzene-d_6) δ 6.35 ("t", J_{HH} = 2.5 Hz, 2 H), 6.15 ("t", J_{HH} = 2.5 Hz, 2 H), 3.03 (t, $^1J_{YH}$ = 35.3 Hz, 2 H), 2.10 (s, 6 H), 2.04 (s, 6 H), 1.31–1.15 (m, 4 H), 1.05 (t, $^3J_{HH}$ = 7.7 Hz, 6 H); IR (Nujol, cm^{-1}) 2910 vs, 2725 w, 1460 vs, 1377 s, 1320 m, 1212 br s, 1172 m, 1128 w, 1062 w, 1041 m, 1012 m, 968 w, 900 m, 888 sh,

(16) Rausch, M. D.; Moriarty, K. J.; Atwood, J. L.; Weeks, J. A.; Hunter, W. E.; Brittain, H. G. *Organometallics* **1986**, *5*, 1281–1283 $(Cp'_2CeCl)_2$.

m, 818 w, 789 s, 749 w, 727 m, 708 m, 610 m, 503 m, 431 m. Anal. Calcd for $C_{36}H_{54}Si_2Y_2$: C, 59.99; H, 7.55. Found: C, 59.88; H, 7.60.

($Et_2SiCpCp''Lu)_2(\mu$-H)(μ-C_2H_5) (17). A 30-mL flask was charged with 0.30 g (0.33 mmol) of **13**. On the vacuum line, toluene was condensed into the flask in vacuo at −78 °C, and the vessel was backfilled with 1 atm of ethylene. The reaction mixture was stirred for 6 h at room temperature and was then filtered. The solvent was removed from the filtrate, and the resulting white solids were washed with 2 × 5 mL of cold pentane: yield 0.22 g (73%); ^{1}H NMR (toluene-d_8, 20 °C) δ 6.19 (m, 2 H), 6.10 (m, 2 H), 5.96 (m, 2 H), 5.87 (m, 2 H), 5.02 (s, 1 H), 2.15 (s, 6 H), 2.08 (s, 6 H), 2.02 (s, 6 H), 1.93 (s, 6 H), 1.29–0.95 (m, 20 H), 0.25 (t, J_{HH} = 7.9 Hz, 3 H); for details of the Lu–CH_2 resonances in **17–21**, see Results section; IR (KBr, cm^{-1}) 2955 s, 2852 s, 1446 m, 1384 w, 1363 m, 1324 s, 1273 br s, 1246 sh, 1180 m, 1067 w, 1042 s, 1011 s, 859 w, 787 s, 751 m, 710 s, 670 m, 656 m, 618 w, 493 s. Anal. Calcd for $C_{38}H_{57}Lu_2Si_2$: C, 49.61; H, 6.25. Found: C, 49.55; H, 6.12.

($Et_2SiCpCp''Lu)_2(\mu$-D)(μ-2-d_1-C_2H_4D) (17-*d*-2-*d*$_1$) was synthesized in a manner analogous to **17** from **13-*d*** and ethylene. The IR spectrum in KBr is essentially identical with the spectrum reported above for **10** except for the absence of a peak at 1273 cm^{-1} and the presence of a new peak at 920 cm^{-1}.

($Et_2SiCpCp''Lu)_2(\mu$-H)(μ-$^{13}CH_2{}^{13}CH_3$) (17-*1,2*-$^{13}C_2$) was synthesized in an NMR tube by treating **13** with $^{13}CH_2{}^{13}CH_2$ in toluene-d_8: ^{13}C NMR (toluene-d_8, 20 °C) δ 32.7 (td, $^1J_{CH}$ = 106 Hz, $^1J_{CC}$ = 25 Hz), 11.6 (qdt, $^1J_{CH}$ = 125 Hz, $^1J_{CC}$ = 25 Hz, $^2J_{CH}$ = 6.5 Hz). This ^{13}C NMR spectrum does not change significantly between −60 °C and +70 °C.

($Et_2SiCpCp''Y)_2(\mu$-H)(μ-C_2H_5) (18) and ($Et_2SiCpCp''Y)_2(\mu$-H)(μ-$^{13}CH_2{}^{13}CH_3$) (18-*1,2*-$^{13}C_2$) were synthesized in NMR tube reactions by treating **14** with ethylene and $^{13}CH_2{}^{13}CH_2$, respectively, in toluene-d_8: ^{1}H NMR (toluene-d_8, 20 °C) δ 6.21 (m, 2 H), 6.17 (m, 2 H), 6.03 (m, 2 H), 5.91 (m, 2 H), 2.34 (t, $^1J_{YH}$ = 38.4, 1 H), 2.16 (s, 6 H), 2.07 (s, 6 H), 2.02 (s, 6 H), 1.92 (s, 6 H), 1.31–0.91 (m, 20 H), 0.21 (t, J_{HH} = 7.6 Hz, 3 H); ^{13}C NMR (toluene-d_8, 20 °C) δ 28.1 ("tq", $^1J_{CH}$ = 107 Hz, $^1J_{YC} \approx {}^1J_{CC} \approx$ 24 Hz), 11.6 ("qqt", $^1J_{CH}$ = 125 Hz, $^2J_{YC} \approx {}^1J_{CC} \approx$ 24 Hz, $^2J_{CH} \sim$ 7 Hz). This spectrum does not appreciably change over the range −65 °C to +70 °C.

($Et_2SiCpCp''Lu)_2(\mu$-H)(μ-*n*-C_3H_7) (19). The procedure described above for the synthesis of ($Et_2SiCpCp''Lu)_2(\mu$-H)(μ-C_2H_5) (**17**) was repeated with 0.18 g (0.19 mmol) of **13** under 1 atm of propylene: yield 0.12 g (68%) of an off-white powder.

($Et_2SiCpCp''Y)_2(\mu$-H)(μ-*n*-C_3H_7) (20). A solution of 0.10 g (0.13 mmol) of **14** in toluene (10 mL) was stirred under 1 atm of propylene for 1 day. The solvent was then removed in vacuo, and the resulting white solids were collected in the glovebox. ^{1}H NMR (toluene-d_8, 16 °C) δ 6.18 (m, 4 H), 6.14 (m, 2 H), 5.90 (m, 2 H), 2.40 (t, $^1J_{YH}$ = 38.2 Hz), 2.17 (s, 6 H), 2.07 (s, 12 H), 1.94 (s, 6 H), 1.33–0.85 (m, 20 H), 0.32 (m, 1 H), −0.71 (m, 1 H); IR (Nujol, cm^{-1}) 2930 vs, 2730 w, 1450 s, 1382 s, 1338 m, 1275 br s, 1172 w, 1047 m, 1020 s, 971 m, 792 m, 783 s, 751 m, 721 m, 672 m, 641 w.

($Et_2SiCpCp''Lu)_2(\mu$-H)(μ-*n*-C_6H_{13}) (21). In the glovebox, a 30-mL flask was charged with 0.12 g (0.12 mmol) of **13**, 10 mL of toluene, and 0.5 mL of 1-hexene (300-fold excess). The solution was stirred for 2 days at room temperature, at which time the volatiles were removed, leaving a viscous, colorless oil. Pentane (5 mL) was then added to the flask in order to triturate the oil, the solvent was removed in vacuo, and the resulting off-white solids were collected in the glovebox: yield 0.11 g (93%); ^{1}H NMR (toluene-d_8, 19 °C) δ 6.24 (m, 2 H), 6.15 (m, 2 H), 6.06 (m, 2 H), 5.87 (m, 2 H), 5.19 (s, 1 H), 2.21 (2, 6 H), 2.10 (s, 6 H), 2.06 (s, 6 H), 1.99 (s, 6 H), 1.32–0.85 (m), −0.18 (m, 1 H); IR (Nujol, cm^{-1}) 2920 vs, 2845 vs, 1455 s, 1378 s, 1327 s, 1282 br s, 1140 w, 1181 m, 1172 m, 1041 s, 1018 s, 939 w, 843 w, 782 s, 750 m, 712 s, 671 s, 568 m, 648 m, 614 m, 489 m. Anal. Calcd for $C_{42}H_{65}Lu_2Si_2$: C, 51.68; H, 6.71. Found: C, 51.49; H, 6.53.

NMR Kinetic and Equilibration Experiments. In a typical kinetics experiment, a 5-mm NMR tube equipped with a Teflon valve was charged in the glovebox with 0.700 mL of a toluene-d_8 solution of lanthanide complex **13** and 10.0–50.0 μL of 1-hexene (solution transfers were made with Hamilton precision syringes). The quantity of 1-hexene was at least 15 times in molar excess, as required to maintain pseudo-zero-order reaction conditions in olefin.[17] The NMR tube was shaken, and an initial spectrum (t = 0) was recorded. The sample was then immersed in a thermostated Haake constant temperature bath, controllable to ±0.2 °C. At appropriate time intervals, the sample tube was removed from the oil bath and cooled to −78 °C. The ^{1}H NMR spectrum was then recorded at room temperature, and the sample was returned to the oil bath. A long pulse delay (≥5 T_1) was used in NMR data acquisition. From extrapolation of the kinetic data, it was determined that negligible reaction occurs at room temperature during the time necessary (≤15 min) to record the NMR spectrum. The kinetics were monitored by following the difference in intensity between a product Cp signal and the sum of a coincident product Cp and a starting M–H signal; these signals are all relatively close in chemical shift (only a 0.3 ppm chemical shift range) so that electronic integration of these peaks was both straightforward and precise. For the kinetic run at 45 °C, rate constant data were also calculated by measuring changes in the area of one starting material (**13**) Cp peak and product (**21**) μ-hydride peak, which are well-separated; these data exhibited slightly more scatter, but essentially the same rate constants were derived by using either method. The kinetics were followed for at least 3 half-lives. The data for these reactions could be fit by least-squares analysis to eq 1, where C_0 is the

$$\ln (C_0/C) = k't \quad (1)$$

initial concentration of the hydride compound (measured as the sum of the starting material and product peaks) and C is the concentration of product. Standard deviations are derived from the fitting procedure. Olefin concentrations were corrected for loss of olefin to the vapor phase and were calculated by using tabulated vapor pressures[18] and densities[19] for both 1-hexene and toluene and by using Raoult's law for an ideal solution;[20] in no case were corrections greater than 5%. Control experiments, consisting of the heating solutions of either **13** or **21** in toluene-d_8, indicate that exchange of the solvent deuterons into either the hydride peak of **13** or the Cp peaks of either **13** or **21** does not occur at any appreciable rate at the temperatures used in these studies.

The equilibrium constant for eq 13 was measured as a function of temperature by monitoring the Cp region as described above, after samples of **13** and 1-hexene in toluene-d_8 had relaxed to equilibrium (≥10 half-lives). These measurements were taken on two independently prepared samples, consisting of the hydride dissolved in toluene-d_8 and 20.0 μL of 1-hexene, sealed in 5-mm NMR tubes. The concentration of 1-hexene in solution was calculated as described above.

Olefin Hydrogenation and Polymerization Studies. Olefin hydrogenation rates were measured by using simple vacuum line/mercury manometer techniques and were found not to be rapid enough to be influenced by mass transport effects.[3b] In a typical ethylene polymerization experiment, 20 mg of the catalyst of interest was charged in a 100-mL flask. On the vacuum line, ca. 20–25 mL of toluene was condensed into the flask in vacuo, and the flask was warmed to room temperature and then filled with 1 atm of ethylene. The reaction mixture was maintained under 1 atm of ethylene, stirred vigorously for a measured time interval, and was then quenched with methanol. The polyethylene formed was collected by filtration, washed with acetone, and dried in vacuo for at least 2 h before weighing.

X-ray Crystallographic Studies. All diffraction experiments were performed on an Enraf-Nonius CAD4 diffractometer at −120 °C with Mo Kα radiation. The structure determinations were carried out on a MicroVAX 3600 computer employing the TEXSAN crystallographic software package.[21] Atomic scattering factors were those tabulated by Cromer and Waber[22] with anomalous dispersion corrections being applied to the nonhydrogen atoms.[23]

X-ray Crystallographic Study of $Me_2SiCpCp''LuCH(SiMe_3)_2$ (4). Colorless crystals of **4** were grown by simultaneous solvent removal and cooling of a saturated pentane solution and were sealed in glass capillaries. Crystal data collection parameters are listed in Table I. Preliminary measurements and cell reduction calculations (TRACER) showed that the compound crystallizes in the triclinic space group $P\bar{1}$ (no. 2). Intensities of four standard reflections were measured every 3 h of X-ray exposure and showed no significant variations. Intensity data were corrected for Lorentz and polarization effects. An empirical absorption correction based on ψ scans of six reflections was applied. The transmission factors were in the range 0.78–1.00. The structure was solved

(17) Moore, J. W.; Pearson, R. G. *Kinetics and Mechanism*, 3rd ed.; John Wiley: New York, 1981; Chapter 2.

(18) (a) Dreisbach, R. R. *Adv. Chem. Ser.* **1959**, *15*, 12. (b) Reference 18a, Vol. 22, p 229.

(19) Riddick, J. A.; Bunger, W. B.; Sakano, T. K. *Organic Solvents—Physical Properties and Methods of Purification*; Wiley: New York, 1986; Vol. II, pp 168–169, 137–138.

(20) (a) The thermodynamic properties of vapor–liquid equilibria for the toluene–1-hexene binary system have been investigated.[20b] These studies reveal a very small excess Gibbs energy, and thus relatively ideal Raoult's Law behavior, for this solvent system. (b) Vera, J. H.; Prausnitz, J. M. *J. Chem. Eng. Data* **1971**, *16*, 149–154.

(21) Swepston, P. N. TEXSAN Crystallographic Program Package; Molecular Structure Corp.: College Station, TX, 1986.

(22) Cromer, D. T.; Waber, J. T. *International Tables for X-ray Crystallography*; The Kynoch Press: Birmingham, England, 1974; Vol. IV, p 98.

(23) Reference 22, pp 149–150.

Table I. Crystallographic Details for $Me_2SiCpCp''LuCH(TMS)_2$ (4), $(Et_2SiCpCp''LuH)_2$ (13), and $(Et_2SiCpCp''Lu)_2(H)(C_2H_5)$ (17)

complex	$Me_2SiCpCp''LuCH(TMS)_2$ (4)	$(Et_2SiCpCp''LuH)_2$ (13)	$[(Et_2SiCpCp''Lu)_2(H)(C_2H_5)]$ (17)
formula	$C_{23}H_{41}Si_3Lu$	$C_{36}H_{54}Si_2Lu_2$	$C_{38}H_{58}Si_2Lu_2$
M	576.80	892.92	920.98
cryst size, mm	0.32 × 0.28 × 0.22	0.41 × 0.29 × 0.25	0.35 × 0.30 × 0.24
cryst system	triclinic	monoclinic	monoclinic
space group	$P\bar{1}$ (no. 2)	$P2_1/n$ (no. 14)	$P2_1/c$ (no. 14)
a, Å	16.049 (3)	11.558 (3)	11.679 (4)
b, Å	17.945 (4)	8.590 (2)	25.755 (5)
c, Å	8.993 (3)	18.029 (3)	18.074 (2)
α, deg	93.36 (2)	90	90
β, deg	90.92 (2)	100.10 (2)	99.41 (2)
γ, deg	82.54 (2)	90	90
V, Å^3	2564 (2)	1762 (1)	5363 (4)
z	4	2	6
d_{calcd}, g cm^{-3}	1.49	1.68	1.71
μ (Mo Kα), cm^{-1}	40.01	56.68	55.89
temp (°C)	−120	−120	−120
radiation	graphite-monochromated Mo Kα (λ = 0.71069 Å)		
scan type	$2\theta/\theta$	$2\theta/\theta$	ω
2θ, deg	4–48	4–55	4–50
scan width, deg	0.8 + 0.35 tan θ	0.85 + 0.35 tan θ	1.0 + 0.35 tan θ
unique data	8024	4315	7820
unique data with $I > 3\sigma(I)$	6085	2656	4643
no. of parameters	813	289	357
R(F)	0.030	0.022	0.058
R_w(F)	0.036	0.030	0.069
GOF	1.75	1.02	1.69

by direct methods (MITHRIL).[24] Full-matrix least-squares refinement with anisotropic thermal parameters for all non-hydrogen atoms of the two independent molecules found in the unit cell yielded a final R(F) of 0.030 (R_w(F) = 0.036). All hydrogen atoms were located from difference Fourier maps and were refined with isotropic temperature factors. The H4B and H20B1 atoms were characterized by slightly negative temperature factors and in the last cycle of the refinement were given fixed B_{iso} values. The final difference Fourier map revealed a peak 1.45 eÅ^{-3} high located near one of the Lu atoms.

X-ray Crystallographic Study of $(Et_2SiCpCp''LuH)_2$ (13). Single crystals of **13** were grown by allowing hydrogen to diffuse into an undisturbed solution of **5** in pentane. The colorless prisms were isolated by decantation and sealed in glass capillaries. Crystal and data collection information are given in Table I. Intensities of three standard reflections were monitored every 3 h of X-ray exposure and showed no significant variations. The data were corrected for Lorentz-polarization and empirical absorption effects (ψ scans of eight reflections, transmission factors range 0.89–1.00). The structure was solved by heavy atom techniques (Patterson and Fourier maps). Full-matrix least-squares refinement with anisotropic thermal parameters for all non-hydrogen atoms gave the final R(F) of 0.022 and R_w(F) = 0.030. All hydrogen atoms were found from Fourier difference maps and refined with isotropic thermal parameters. The highest peak (2.13 eÅ^{-3}) in the final electron density map was located near the Lu atom.

X-ray Crystallographic Study of $(Et_2SiCpCp''Lu)_2(\mu\text{-}H)(\mu\text{-}C_2H_5)$ (17). Crystals of **17** were grown by concurrent slow cooling and solvent evaporation from a saturated toluene solution and sealed in glass capillaries. Lattice parameters were determined by least-squares techniques applied to setting angles of 25 high-angle reflections. The systematic absences uniquely indicated the monoclinic space group $P2_1/c$ (no. 14). The intensities of three standard reflections were monitored every 3 h of X-ray exposure and showed no significant decay. The data were corrected for Lorentz and polarization effects. Empirical absorption corrections using DIFABS[21] were applied with transmission factors in the range 0.81–1.24. The crystal diffracted rather weakly. The structure was solved by direct methods in SHELX86. The structure analysis revealed that there are two crystallographically different molecules of the complex in the unit cell. One hydridoalkyl molecule occupies the general positions, while another molecule is disposed around the center of symmetry. During the latter stage of the structure determination, two higher peaks ca. 1.5 Å apart were found in the region between the Lu atoms of the second molecule. It was then assumed, in good agreement with the NMR data, that this site represents an overlap of positionally disordered hydridoalkyl species. The two bridging carbon atoms were therefore refined with the occupancy factors of 0.5. Refinement was performed by full-matrix least-squares procedures with anisotropic thermal parameters for the Lu, Si, and C atoms of both the bridging alkyl group (molecule 1) and the diethylsilyl side chains. The final R factor was 0.058 (R_w(F) = 0.069) for 4643 reflections with $I > 3\sigma(I)$ and 357 parameters. The largest peak in the final difference map (2.12 eÅ^{-3}) was located near the Lu3 atom.

(24) Gilmore, G. N. MITHRIL: A computer program for the automatic solution of crystal structure from X-ray data; University of Glasgow, Scotland, 1983.

Results

We begin with remarks on ligand synthesis, followed by the synthesis of halo precursors and $CHTMS_2$ derivatives. Next, the crystal structure of $Me_2SiCpCp''LuCHTMS_2$ is compared and contrasted with those of the more coordinatively saturated Cp'_2 and $Me_2SiCp''_2$ analogues. The hydrogenolytic reactivity of $R_2SiCpCp''MCHTMS_2$ complexes is then discussed, along with the unusual molecular structure of the hydrogenolysis product $(Et_2SiCpCp''LuH)_2$. A reactivity study of these $(\mu\text{-}H)_2$ compounds includes a kinetic and thermodynamic analysis of the α-olefin chemistry as well elucidation of the molecular structure of the insertion product $(Et_2SiCpCp''Lu)_2(\mu\text{-}H)(\mu\text{-}C_2H_5)$. The final topic concerns the unusual molecular dynamics and reactivity of this type of organolanthanide μ-alkyl.

Ligand Synthesis. The preparation of $R_2Si(CpH)(Cp''H)$ (R = Me, Et) and subsequent conversion to the corresponding crystalline lithium salts is shown in eqs 2 and 3. Overall isolated yields of these air-sensitive reagents are high (70–90%). Although THF can be removed by prolonged heating and pumping, the higher crystallinity of the final THF adducts renders them more amenable to purification.

$$Cp''H \xrightarrow[(2)\ R_2SiCl_2]{(1)\ n\text{-BuLi}} R_2SiCp''Cl \qquad (2)$$

$$Cp''SiR_2Cl \xrightarrow[(2)\ 2n\text{-BuLi}]{(1)\ NaCp} R_2SiCpCp''Li_2{\cdot}2THF \quad R = Me,Et \qquad (3)$$

Organolanthanide Halo Precursors and Hydrocarbyls. Lutetium and yttrium halo complexes of the $R_2SiCpCp''$ ligands were prepared as shown in eq 4. Exchange of diethyl ether for THF yields products which are more crystalline and less susceptible

$$MCl_3 + R_2SiCpCp''Li_2{\cdot}2THF \xrightarrow[(2)\ \text{ether}]{(1)\ THF} R_2SiCpCp''MCl^-Li(ether)_2^+ + 2LiCl \qquad (4)$$

1, R = Me; M = Lu
2, R = Et; M = Lu
3, R = Et; M = Y

to undesired side reactions (e.g., reaction of THF with lithium reagents). Complexes **1–3** were characterized by standard ana-

lytical and spectroscopic techniques (see Experimental Section); they are assigned pseudotetrahedral structure D, for which there is considerable precedent.[1,2,25,26]

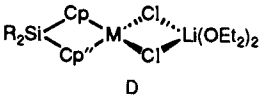

D

Alkylation of the halo compounds proceeds smoothly in toluene to afford the pentane soluble hydrocarbyls, **4–6** (eq 5). These alkyls are colorless, crystalline, and exceedingly air- and moisture-sensitive. They are stable at room temperature both in the

$$R_2SiCpCp''MCl_2^-Li(ether)_2^+ + LiCH(TMS)_2 \xrightarrow{\text{toluene}} \underset{\textbf{1-3}}{} R_2SiCpCp''MCH(TMS)_2 + 2LiCl + 2ether \quad (5)$$

4, R = Me; M = Lu
5, R = Et; M = Lu
6, R = Et; M = Y

solid state and in hydrocarbon solutions for months. ^{1}H- (e.g., Figure 1 (supplementary material)[27]) and ^{13}C-NMR spectra at room temperature (see Experimental Section for data) reveal C_s symmetry for the Me_4C_5, C_5H_4(AA'BB'), and Me_2Si/Et_2Si moieties as well as magnetically equivalent Si–Me units. These results suggest conformation E or F, while the small magnitude of methine $^1J_{CH}$ (~93 Hz) and the methine proton coupling to ^{89}Y ($^2J_{Y-H}$ = 2.5 Hz; Figure 1B) are suggestive of M–C–H "agostic" interactions.[3,6a,28,29] This feature and conformation E are confirmed by the diffraction results (vide infra). Variable-temperature ^{1}H-NMR studies reveal equivalence of $CHTMS_2$ Si–Me groups to −80 °C. As for the Cp'_2 and $Me_2SiCp''_2$ analogues,[3] permutation of structurally nonequivalent Si–Me groups (vide infra) occurs with a low barrier.

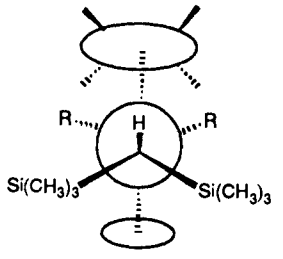

E

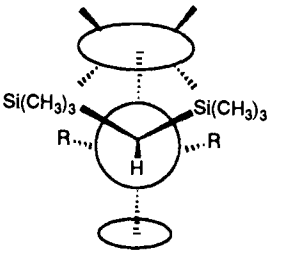

F

Molecular Structure of $(CH_3)_2Si[C_5H_4][(CH_3)_4C_5]LuCH[Si(CH_3)_3]_2$ (4). Low-temperature structural analysis reveals that crystals of **4** are composed of two crystallographically independent molecules per unit cell. Only one of the two independent molecules is discussed, since the two have nearly identical structures. The high quality of the data allowed solution and refinement of all except two H atom positions (see Experimental Section) and provide more precise definition of certain unusual organolanthanide structural features than has previously been possible. Final atomic coordinates and anisotropic thermal parameters are given in Tables II and III in the supplementary material,[27] using the labeling scheme of Figure 2. Important bond lengths and angles are given in Table IV and in the supplementary material.

The coordination pattern about lutetium in **4** is of the Cp'_2MX "bent-sandwich" type and is roughly similar to other crystallographically characterized organolanthanide metallocenes with $CHTMS_2$ ligation, namely $Cp'_2LnCHTMS_2$ (Ln = Ce[30] (**7**), Nd[31] (**8**), and Y[28b] (**9**)) and $Me_2SiCp''_2NdCHTMS_2$[3a] (**10**). As a consequence of the Me_2Si bridge in **4**, the ring centroid–Lu–ring centroid angle has contracted from 134–140° usually seen in Cp'_2-based organolanthanides (134.4° in **9**) to 125.2°. This effect is also observed in going from **8** to **10** (134.4° versus 121.3°) and from $Cp'_2Th(CH_2TMS)_2$[32] to $Me_2SiCp''_2Th(CH_2TMS_2)_2$[4] (**11**) (134.9° versus 118.4°). In the present case, the C_g–Lu–C_g angle probably reflects a compromise between induced strain at Si1 (deviations from tetrahedral geometry, vide infra) and maximizing η^5-Cp, -Cp'' coordination to Lu; that this angle is smaller in **4** than for either **10** or **11** most likely due to the smaller ionic radius of Lu^{3+}.[33] The strain at Si1 is evident in the acute ∠C3–Si1–C8

Table IV. Selected Bond Lengths (Å) and Angles (deg) in Coordination Groups of $Me_2SiCpCp''LuCH(TMS)_2$ (**4**)

Bond Lengths			
Lu–C17	2.365 (7)	Si2–C18	1.864 (9)
Lu–C19	2.820 (8)	Si2–C19	1.910 (8)
Lu–C3	2.568 (6)	Si2–C20	1.862 (8)
Lu–C4	2.581 (7)	Si3–C17	1.827 (7)
Lu–C5	2.651 (7)	Si3–C21	1.866 (8)
Lu–C6	2.641 (7)	Si3–C22	1.868 (9)
Lu–C7	2.580 (7)	Si3–C23	1.875 (8)
Lu–C8	2.526 (7)	C3–C4	1.42 (1)
Lu–C9	2.553 (7)	C3–C7	1.42 (1)
Lu–C10	2.640 (6)	C4–C5	1.40 (1)
Lu–C11	2.663 (7)	C5–C6	1.39 (1)
Lu–C12	2.561 (7)	C6–C7	1.40 (1)
Lu–H17	2.58 (6)	C8–C9	1.44 (1)
Lu–H191	2.74 (9)	C8–C12	1.432 (9)
Lu–H192	2.74 (11)	C9–C10	1.43 (1)
Si1–C1	1.85 (1)	C10–C11	1.41 (1)
Si1–C2	1.87 (1)	C10–C14	1.49 (1)
Si1–C3	1.863 (7)	C11–C12	1.41 (1)
Si1–C8	1.874 (7)	C11–C15	1.48 (1)
Si2–C17	1.813 (7)	C12–C16	1.52 (1)
Si2–C18	1.864 (9)	C17–H17	0.81 (6)
C19–H191	1.08 (10)	C19–H192	0.88 (11)
C19–H193	1.03 (8)		

Bond Angles			
C3–Lu–C8	87.2 (2)	C6–C7–C3	109.5 (7)
C1–Si1–C2	108.4 (5)	C4–C3–C7	104.5 (6)
C1–Si1–C3	112.0 (4)	C8–C9–C10	108.3 (6)
C1–Si1–C8	112.8 (4)	C9–C10–C11	108.1 (6)
C2–Si1–C3	109.3 (4)	C10–C11–C12	108.2 (6)
C2–Si1–C8	115.1 (4)	Lu–C17–Si2	97.7 (3)
C3–Si1–C8	98.9 (3)	Lu–C17–Si3	126.2 (3)
C17–Si2–C18	114.4 (4)	Lu–C17–H17	96 (4)
C17–Si2–C19	107.5 (3)	Si2–C17–Si3	123.6 (4)
C17–Si2–C20	114.7 (4)	H191–C19–H193	104 (6)
C17–Si3–C21	113.8 (4)	H192–C19–H193	102 (8)
C17–Si3–C22	111.2 (4)	H191–C19–H192	109 (8)
C17–Si3–C23	111.3 (4)	C_g–Lu–C_g''[a]	125.2
Si1–C3–C4	123.6 (5)		
Si1–C3–C7	126.5 (5)		
Si1–C8–C9	125.9 (5)		
Si1–C8–C12	123.3 (5)		
C3–C4–C5	110.0 (7)		
C4–C5–C6	107.4 (7)		
C5–C6–C7	108.5 (7)		
C6–C7–C3	109.5 (7)		

[a] Cg and Cg'' = ring centroids.

(25) (a) Tilley, T. D.; Andersen, R. A.; Zalkin, A. *Inorg. Chem.* **1983**, *22*, 856–859. (b) Tilley, T. D.; Andersen, R. A. *Inorg. Chem.* **1981**, *20*, 3267–3270.

(26) (a) Watson, P. L.; Whitney, J. F.; Harlow, R. L. *Inorg. Chem.* **1981**, *20*, 3271–3278. (b) Lappert, M. F.; Singh, A.; Atwood, J. L.; Hunter, W. E. *J. Chem. Soc., Chem. Commun.* **1981**, 1191.

(27) See paragraph at end of paper regarding supplementary material.

(28) (a) Bruno, J. W.; Smith, G. M.; Marks, T. J.; Fair, C. K.; Schultz, A. J.; Williams, J. M. *J. Am. Chem. Soc.* **1986**, *108*, 40–56. (b) den Haan, K. H.; Baer, J. L.; Teuben, J. H.; Spek, A. L.; Kojić-Prodić, B.; Hays, G. R.; Huis, R. *Organometallics* **1986**, *5*, 1726–1733. (c) As noted in ref 3a, C(α) valence angles and hybridization in $MCHTMS_2$ complexes must also reflect the prodigious bulk of the TMS substituents. Such effects have been observed in the parent alkylsilanes: Eaborn, C.; El-Kheli, M. N. A.; Hitchcock, P. B.; Smith, J. D. *J. Organomet. Chem.* **1984**, *272*, 1–9, and references therein.

(29) (a) Cotton, F. A.; Luck, R. L. *Inorg. Chem.* **1989**, *28*, 3210–3213, and references therein. (b) Brookhart, M.; Green, M. L. H.; Wong, L.-L. *Prog. Inorg. Chem.* **1988**, *36*, 1–124, and references therein. (c) Crabtree, R. H.; Hamilton, D. G. *Adv. Organomet. Chem.* **1988**, *28*, 299–338, and references therein.

(30) Heeres, H. J.; Renkema, J.; Booij, M.; Meetsma, A.; Teuben, J. H. *Organometallics* **1988**, *7*, 2495–2502.

(31) Jeske, G.; Lauke, H.; Mauermann, H.; Swepston, P. N.; Schumann, H.; Marks, T. J. *J. Am. Chem. Soc.* **1985**, *107*, 8091–8103.

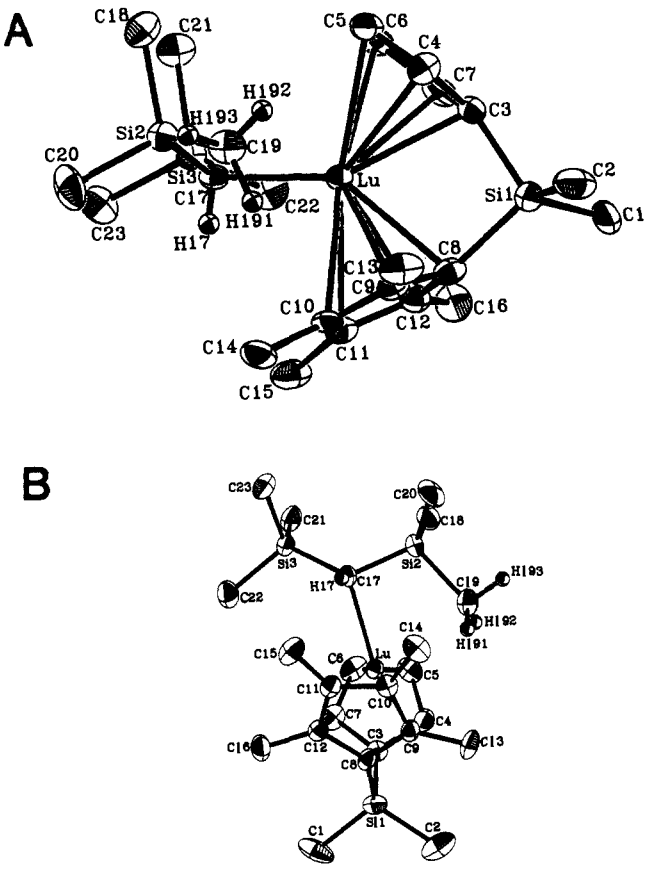

Figure 2. (A) Perspective ORTEP drawing of the molecular structure of $Me_2SiCpCp''LuCH(TMS)_2$ (**4**). Only selected hydrogen atoms are shown. All non-hydrogen atoms are represented by thermal vibrational ellipsoids drawn to encompass 50% probability. (B) Another perspective ORTEP view of the molecular structure of $Me_2SiCpCp''LuCH(TMS)_2$ (**4**). Only selected hydrogen atoms are shown. All non-hydrogen atoms are represented by thermal vibrational ellipsoids drawn to encompass 50% probability.

= 98.9 (3)° (versus 101.0 (3)° in **10**, and 100.6 (9)° in **11**); also, Si1 is displaced from the C_5 mean ring planes in the direction of Lu by 0.63 Å (C_5H_4) and 0.57 Å (C_5Me_4) (versus 0.41 Å in **10**). As was seen in both the $Me_2SiCp''_2$, Nd (**10**) and Th (**11**) systems, the Lu–C(ring) distances exhibit significant dispersion, with the longest being to C atoms farthest from Si1 (i.e., 2.651 (7) Å (Lu–C5), 2.641 (7) Å (Lu–C6), 2.640 (6) Å (Lu–C10), and 2.663 Å (Lu–C11) versus 2.568 (6) Å (Lu–C3) and 2.526 (7) Å (Lu–C8)). The lutetium ion is equidistant from both the C_5H_4 and the Me_4C_5 rings, with average Lu–C distances of 2.60 (4, 3, 5, 5) Å[34] and 2.59 (6, 6, 7, 5) Å, respectively. The internal ring dimensions in both rings are unexceptional. Thus, the average C–C(ring) = 1.41 (1, 1, 2, 5) Å for C_5H_4 and 1.42 (1, 1, 2, 5) Å for Me_4C_5, and the average C–CH_3 = 1.50 (2, 1, 2, 4) Å.

The decreased interligand steric demands of $Me_2SiCpCp''$ versus Cp'_2 ligation in **4** allow closer approach of the hydrocarbyl fragment, which is particularly evident in the metal–carbon σ bond distance. Thus, Lu–C(17) = 2.365 (7) Å, whereas for $Cp'_2YCHTMS_2$ (**9**), this distance is 2.468 (7) Å (correcting for differences in Lu^{3+} and Y^{3+} eight-coordinate ionic radii,[33] Y–C in **9** is predicted to be 2.426 (7) Å). The present Lu–C σ bond distance is in better agreement with Ln–C distances seen for earlier, larger lanthanides where steric repulsions of the Cp′ and hydrocarbyl ligands are more easily accommodated. Correcting for differences in lanthanide ionic radii, Ce–C in **7** becomes 2.369 (5) Å for Lu–C (2.535 (5) Å actual), Nd–C in **8** becomes 2.385 (7) Å for Lu–C (2.517 (7) Å actual), and Nd–C in **10** becomes 2.371 (7) Å for Lu–C (2.506 (7) Å actual). Moreover, the distance in **4** is not unusual for a lutetium–carbon σ bond involving a less bulky alkyl group; the terminal metal–CH_3 bond length in $Cp'_2Lu(\mu\text{-}CH_3)LuCp'_2(CH_3)$ is 2.344 (12) Å.[2g]

The $CHTMS_2$ coordination in **4** also involves a highly unsymmetrical, secondary Lu–hydrocarbyl interaction (Lu···C(19)H_3, Figure 2B). Qualitatively similar but metrically different interactions are observed in other Ln–$CHTMS_2$ complexes (e.g., **7**, **8**, **9**, and **10**). Thus, ∠Lu–C17–Si2 in **4** is 97.7 (3)°, which agrees well with those seen in **8**–**10** (e.g., 96.7 (3)° in **9** and 97.1 (3)° in **10**). The present Lu–C17–Si3 angle, 126.2 (3)°, is also distorted from tetrahedral geometry, apparently due to nonbonded repulsive interactions between the TMS fragment and the ring system. However, more severe distortions are seen in **8** (138.6 (4)°) and **9** (140.2 (4)°) where the Cp'_2 ligation is more sterically demanding, whereas for the ring-bridged **10**, an angle intermediate between these values is observed (132.4 (4)°). In the present case, the more open coordination sphere in **4** allows displacement of the $SiMe_3$ groups (especially C18 and C21) in the direction *away* from the bulky Me_4C_5 ring (Figure 2). In the case of **7**, **8**, and **10**, the metal, α-carbon, and both $CHTMS_2$ silicon atoms are found to be essentially coplanar. However, for **4**, C17 is 0.40 (1) Å out of the plane defined by Lu, Si2, and Si3; also, this plane intersects the plane formed by C17, Si2, and Si3 with a dihedral angle of 27.5°. The cause of this difference appears to be a combination of relieving steric repulsions and the smaller ionic radius of Lu^{3+}; in **9**, the corresponding α-carbon atom-to-plane distance is 0.248 (8) Å.

The aforementioned "agostic" Lu–CH_3Si interaction in **4** (Figure 2B) is characterized by Lu–C19 = 2.820 (8) Å. Correcting for differences in lanthanide eight-coordinate ionic radii, this Lu–C distance is slightly longer than the 2.751 Å (2.917 (1) Å actual) predicted for **7**, 2.763 Å (2.895 (7) Å actual) predicted for **8**, 2.730 Å (2.862 (8) Å actual) predicted for **10**, and 2.759 Å (2.878 (8) Å actual) predicted for **9**. The close Lu–(C19)H_3 interaction in **4** is accompanied by a significant lengthening of the corresponding Si–C19 bond distance. Thus, C19–Si2 = 1.910 (8) Å, which can be compared to C18–Si2 = 1.864 (9) Å, C20–Si2 = 1.862 (8) Å, and C(methyl)–Si(av) = 1.865 (8, 5, 15, 7) Å.

All of the chemically interesting hydrogen atoms in **4** could be located and were successfully refined. Although the associated metrical parameters must be viewed with appropriate precautions and are clearly no substitute for neutron diffraction data, significant qualitative remarks can be made. The dispositions of hydrogen atoms H191–H193 do not minimize Lu–H distances in any obvious fashion, as in many "agostic" C–H···M structural motifs.[28,29] Rather, the present disposition is reminiscent of three-center, two-electron μ-alkyl groups, as was found in $[Cp_2M(\mu\text{-}CH_3)]_2$[35] (G), $Cp_2M(\mu\text{-}CH_3)_2Al(CH_3)_2$[36] (H), (M = Y, Yb), and $[Cp'_2M(\mu\text{-}CH_3)_2AlMe_2]_2$ (M = Sm,[37] Y^{38}) (I).

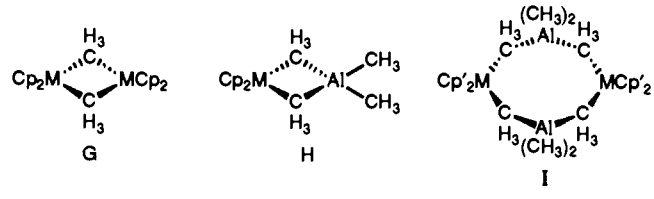

Recent theoretical and PES[39,40] results argue that donation of

(32) Bruno, J. W.; Marks, T. J.; Day, V. W. *J. Organomet. Chem.* **1983**, *250*, 237–246.

(33) (a) Representative eight-coordinate effective ionic radii:[33b] Ce^{3+} (1.143 Å), Nd^{3+} (1.109 Å), Y^{3+} (1.019 Å), Yb^{3+} (0.985 Å), and Lu^{3+} (0.977 Å). (b) Shannon, R. D. *Acta Crystallogr., Sect. A* **1976**, *A32*, 751–767.

(34) The first number in parentheses following an averaged value of a bond length or angle is the root-mean-square estimated standard deviation of an individual datum. The second and third numbers, when given, are the average and maximum deviations from the averaged value, respectively. The fourth number represents the number of individual measurements which are included in the average value.

(35) Holton, J.; Lappert, M. F.; Ballard, D. G. H.; Pearce, R.; Atwood, J. L.; Hunter, W. E. *J. Chem. Soc., Dalton Trans.* **1979**, 54–61.

(36) Holton, J.; Lappert, M. F.; Ballard, D. G. H.; Pearce, R.; Atwood, J. L.; Hunter, W. E. *J. Chem. Soc., Dalton Trans.* **1979**, 45–53.

(37) Evans, W. J.; Chamberlain, L. R.; Ulibarri, T. A.; Ziller, J. W. *J. Am. Chem. Soc.* **1988**, *110*, 6423–6432.

(38) Busch, M. A.; Harlow, R.; Watson, P. L. *Inorg. Chim. Acta* **1987**, *140*, 15–20.

electron density from the Si–C bonding orbital to the electron-deficient lanthanide center represents a major attractive force in such interactions. In addition to the lengthening of C19–Si2, the present Lu–Si2 distance (3.166 (2) Å) appears to support this contention. Correcting this parameter for the difference in silicon and carbon covalent radii[41] yields a hypothetical Lu–C ≈ 2.77 Å, which is shorter than the observed Lu–C19 distance (2.820 (8) Å). As noted above, NMR results indicate that this structure does not lie in a particularly deep potential well.

$R_2SiCpCp''MCHTMS_2$ Reactivity, Metal–Carbon Bond Hydrogenolysis and Hydride Characterization. Exposure of $Cp'_2MCHTMS_2$ and $Me_2SiCp''_2MCHTMS_2$ solutions to hydrogen results in rapid M–$CHTMS_2$ hydrogenolysis and the formation of the corresponding dimeric hydrides.[3,31] These hydrides have been assigned structures J and K[3,31,42] and are highly

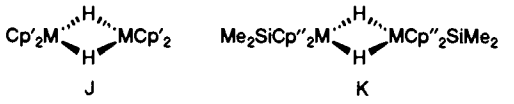

J K

active catalysts for olefin hydrogenation and polymerization/oligomerization.[3,31] In contrast, **4**, **5**, and **6** undergo hydrogenolysis at a rate which is ca. 10^3 slower (eq 6). The products **13** and **14** are sparingly soluble in hydrocarbon solvents, while **12** is completely insoluble in aliphatics. An intermediate is observed in the hydrogenolysis which will be discussed following the molecular structures of **12–14**.

$$\underset{\textbf{4–6}}{R_2SiCpCp''MCH(TMS)_2} + H_2 \xrightarrow{\text{pentane}} \underset{\textbf{[16]}}{[\ \ ]} \rightarrow \tfrac{1}{2}(R_2SiCpCp''MH)_2 + CH_2TMS_2 \quad (6)$$

(quantitative by NMR)

12, R = Me; M = Lu
13, R = Et; M = Lu
13d, MH = MD
14, R = Et; M = Y

^{1}H NMR spectra of **12** and **14** (Figure 3; see Experimental Section for data) are consistent with C_s (on the NMR time scale) dimeric structures, with two Cp″–Me signals, two Cp–H signals (having appropriate AA′BB′ patterns), and appropriate Si–R degeneracies. The M–H resonances occur at relatively low field (e.g., δ 5.87 for **13**), typical of d^0, f^0, and f^{14} hydrides,[1,2] with the ^{89}Y–H coupling pattern in **14** (triplet, $^1J_{Y-H}$ = 35.3 Hz) consistent with symmetrical M(μ-H)$_2$M bridging as in J and K (cf., $[(MeC_5H_4)_2Y(\mu\text{-}H)THF]_2$ where $^1J_{Y-H}$ = 27.2 Hz).[43a,b] While the diffraction results support these deductions, they also indicate that the ancillary ligation is drastically different from that in J and K (vide infra).

Complete IR spectral data for **12–14** and **13-*d*** are collected in the Experimental Section. M–H modes can be identified by subtracting $R_2SiCpCp''$-centered transitions and by comparison with spectra of the deuteride, **13**. Thus, Lu–H (Lu–D) centered modes appear at 1230 (882, ν_{Lu-H}/ν_{Lu-D} = 1.39), 926 (661, ν_{Lu-H}/ν_{Lu-D} = 1.40), and 650 (480, ν_{Lu-H}/ν_{Lu-D} = 1.35) cm^{-1}. The IR spectra for the Y (**14**) and Lu (**13**) derivatives are almost superimposable, suggesting similar molecular structures. These data are compared to analogous hydrides[3,42,43] in Table V. Of note also is the similarity of the IR spectrum of **13** to the corresponding M–H features reported for crystallographically characterized $[Cp'_2Sm(\mu\text{-}H)]_2$.[42] Although the hydrogen atoms were not located, a structure such as J seems probable.[44,45] Also noteworthy is the absence of bands in the region usually assigned to terminal M–H stretching modes ($\gtrsim$1400 cm^{-1}). Thus, IR data also support symmetric M(μ-H)$_2$M structures for **12–14**.

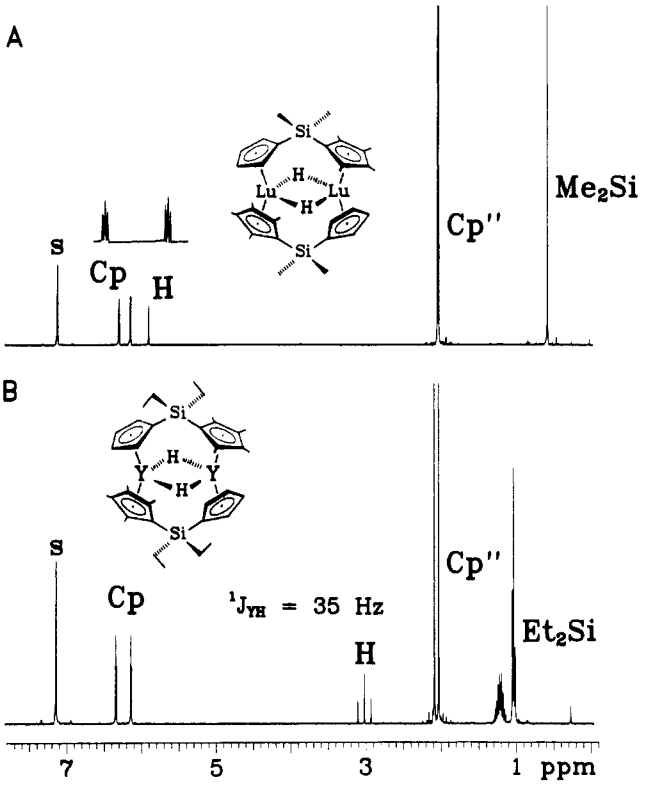

Figure 3. ^{1}H-NMR spectra (400 MHz) of (A) $(Me_2SiCpCp''LuH)_2$ (**12**) and (B) $(Et_2SiCpCp''YH)_2$ (**14**) as solutions in C_6D_6. The s denotes traces of C_6D_5H.

Table V. Metal–Hydride Vibrational Modes for Organolanthanide Hydrides

compound	$\nu_{M-H}(\nu_{M-D})$, cm^{-1}		ref
$(Et_2SiCpCP''LuH)_2$ (**13**)	1230	(882)	this work
	926	(661)	
	650	(480)	
$(Et_2SiCpCp''Lu)_2(\mu\text{-}H)(\mu\text{-ethyl})$ (**17**)	1273	(920)	this work
$[Cp'_2Sm(\mu\text{-}H)]_2$	1140	(820)	42
	940	(660)	
	750	(510)	
$(Cp'_2YH)_2$	1272	(920)	43b
	655	(465)	
$[Cp_2LuH(THF)]_2$	1345	(970)	43c
	945	(677)	
	687	(485)	
$[Me_2SiCp''_2Lu(\mu\text{-}H)]_2$	1120	(820)	3a

Molecular Structure of $\{(C_2H_5)_2Si[C_5H_4][(CH_3)_4C_5]LuH\}_2$ (13). Low-temperature diffraction results for **13** reveal an unusual dimeric structure in which redistribution of the cyclopentadienyl ligation has occurred (Figure 4). The molecule possesses crystallographically imposed C_i symmetry, which relates the two halves of the dimer. Final atomic coordinates and anisotropic thermal parameters are given in Tables VI and VII in the supplementary material,[27] respectively, using the labeling scheme of Figure 4 (starred and unstarred atoms are related by C_i). Important bond

(39) Koga, N.; Morakuma, K. *J. Am. Chem. Soc.* **1988**, *110*, 108–112.
(40) Stern, D.; Nolan, S. P.; Marks, T. J.; Fragalà, I. Manuscript in preparation.
(41) (a) Huheey, J. E. *Inorganic Chemistry*, 3rd ed.; Harper and Row: New York, 1983; pp 256–262. (b) A similar conclusion is reached from van der Waals radii.[41a]
(42) (a) Evans, W. J.; Bloom, I.; Hunter, W. E.; Atwood, J. L. *J. Am. Chem. Soc.* **1983**, *105*, 1401–1403. (b) The Sm–Sm distance in $[Cp'Sm(THF)(\mu\text{-}N_2Ph)]_2$ is 3.491 (2) Å: Evans, W. J.; Drummond, D. K.; Chamberlain, L. R.; Doedens, R. J.; Bott, S. G.; Zhang, H.; Atwood, J. L. *J. Am. Chem. Soc.* **1988**, *110*, 4983–4994.
(43) (a) Evans, W. J.; Meadows, J. H.; Wayda, A. L.; Hunter, W. E.; Atwood, J. L. *J. Am. Chem. Soc.* **1982**, *104*, 2008–2014. (b) Curiously, the ^{1}H spectrum of $(Cp'_2YH)_2$ exhibits a doublet of doublets, suggestive of a static, unsymmetrically bridged structure: den Haan, K. H. Ph.D. Thesis, University of Gröningen, November, 1986. (c) Schumann, H.; Genthe, W.; Hahn, E.; Hossain, M. B.; van der Helm, D. *J. Organomet. Chem.* **1986**, *299*, 67–84.
(44) (a) Saillard, Y.-H.; Hoffmann, R. *J. Am. Chem. Soc.* **1984**, *106*, 2006–2026. (b) Ortiz, J. V.; Hoffmann, R. *Inorg. Chem.* **1985**, *24*, 2095–2104.
(45) Watson, P. L.; Roe, D. C. *J. Am. Chem. Soc.* **1982**, *104*, 6471–6473.

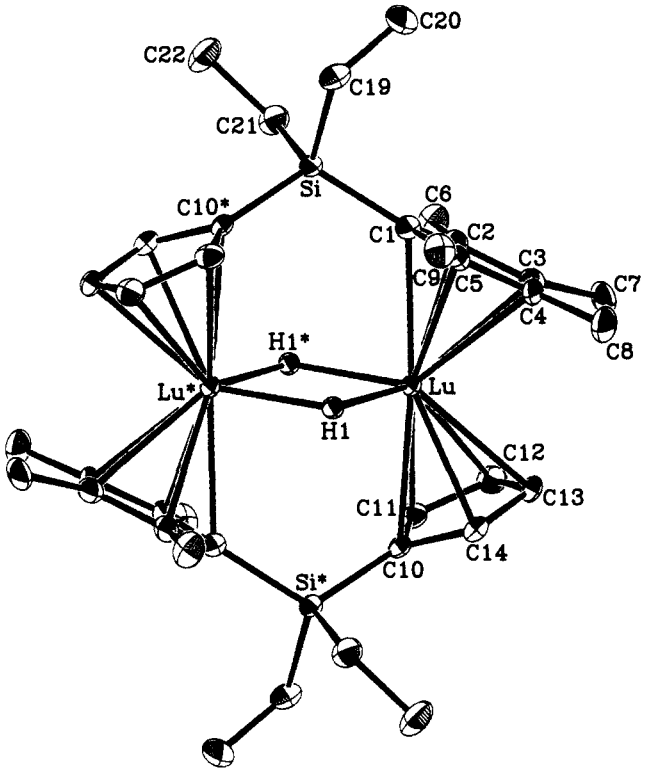

Figure 4. Perspective ORTEP drawing of the molecular structure of $(Et_2SiCpCp''LuH)_2$ (**13**). Only selected hydrogen atoms are shown. All non-hydrogen atoms are represented by thermal vibrational ellipsoids drawn to encompass 50% probability.

Table VIII. Selected Bond Lengths (Å) and Angles (deg) in the Coordination Groups of $(Et_2SiCpCp''LuH)_2$ (**13**)[a]

Lu-C1	2.551 (4)	Si-C10*	1.862 (5)
Lu-C2	2.576 (4)	Si-C19	1.874 (5)
Lu-C3	2.602 (4)	Si-C21	1.880 (5)
Lu-C4	2.613 (5)	C1-C2	1.449 (6)
Lu-C5	2.553 (4)	C1-C5	1.436 (6)
Lu-C10	2.608 (4)	C2-C3	1.413 (6)
Lu-C11	2.601 (5)	C3-C4	1.432 (7)
Lu-C12	2.586 (4)	C4-C5	1.412 (6)
Lu-C13	2.576 (4)	C10-C11	1.428 (6)
Lu-C14	2.566 (4)	C10-C14	1.431 (6)
Lu-H1	2.16 (4)	C11-C12	1.407 (6)
Lu-H1*	2.13 (4)	C12-C13	1.407 (7)
Lu-Lu*	3.390 (1)	C13-C14	1.402 (6)
Si-C1	1.869 (5)	H1-H1*	2.62 (9)
Lu-H1-Lu*	105 (2)	C19-Si-C21	106.5 (2)
H1-Lu-H1*	75 (2)	Cg-Lu-Cg''[b]	132.1
C1-Si-C10*	114.4 (2)		

[a] Starred atoms are related to unstarred atoms by the center of inversion. [b] Cg and Cg'' = ring centroids.

lengths and angles are given in Table VIII.

It can be seen in Figure 4 that the transformation **4** → **13** involves a $2R_2SiCpCp''M \rightarrow M(\mu\text{-}R_2CpCp'')_2M$ rearrangement of the η^5,η^5 ligation. To our knowledge, $(Me_2SiCp_2YbCl)_2$[46] represents the only other f-element example of such a bimetallic "spanning" ligation pattern, and the present results represent the first example where such a structure unambiguously arises from a monometallic precursor. The metrical parameters for **13** (Table VIII) indicate that the coordination geometry of the Lu^{3+} ion is of the bent-sandwich, pseudotetrahedral type, similar to that in numerous other lanthanide, actinide Cp''_2MX_2 complexes.[1-4] In the present spanning ligation, the Lu-C(ring) distances *do not* evidence significant dispersion, in contrast to that seen for $Me_2SiCpCp''$ (**4**) and $Me_2SiCp''_2$ (**10** and **11**) chelation (vide supra). The present internal ring dimensions are unexceptional and are similar to those in **4**. The lutetium ion is again equidistant from the C_5H_4 and C_5Me_4 rings, with average Lu-C distances of 2.58 (2, 1, 2, 5) Å[34] and 2.58 (3, 2, 3, 5) Å, respectively; these values are also very similar to those for $Me_2SiCpCp''$ chelation in **4**. Another consequence of this spanning coordination mode is relief of strain at the bridging silicon atom as compared with **4** and analogues. Thus, ∠C1-Si-C10* is 114.4 (2)°, and the Si is displaced from the C_5 mean ring planes in the direction of Lu by 0.13 Å (C_5H_4) and 0.22 Å (C_5Me_4); these data can be compared to the corresponding angles and distances in **4** of 98.9 (3)°, 0.63 Å, and 0.57 Å. The Cg-M-Cg'' angle also expands from 125° in **4** to 132° in **13**, which is more typical of values seen in Cp'_2MX derivatives.[1-3]

The relatively short Lu-Lu* distance of 3.390 (1) Å in **13** is also noteworthy. It can be compared to Lu-Lu distances of 3.44 and 3.19 Å estimated from twice the lutetium metallic radius[47] (12 coordination) and single bond radius,[48] respectively. Regarding other bis(cyclopentadienyl) hydride systems, the present distance can be compared to a Lu-Lu distance of 3.5216 (6) Å in $[Cp_2LuH(THF)]_2$,[43c] a Sm-Sm distance of 3.905 (3) Å in $[Cp'_2Sm(\mu\text{-}H)]_2$ (J),[42] and the shortest Er-Er distance of 3.684 (1) Å in $\{[(C_5H_5)_2ErH]_3Cl\}\{Li(THF)_4\}$;[49] after correcting for differences in eight- and nine-coordinate ionic radii, these latter two values become 3.701 and 3.514 Å, respectively for Lu^{3+}. Clearly, the metal-metal distance in **13** is substantially shorter. The reason can most plausibly be attributed to the constraints imposed by $M(\mu\text{-}R_2SiCpCp'')_2M$ ligation, and it appears unnecessary to invoke extensive Lu-Lu bonding. An analogous d(M-M) flexibility is evident in the structure of $[Me_2SiCp''_2Th(\mu\text{-}H)_2]_2$,[4a] where the presence of $M(\mu\text{-}H)_4M$ bonding contracts the Th-Th distance (3.632 (2) Å) to ~0.38 Å below that of $[Cp'_2ThH(\mu\text{-}H)]_2$[50] and into the region of twice the metallic radius.[47,48]

Figure 4 also shows the hydrogen atoms bound to lutetium. The quality of the crystals and data collection allowed location and successful refinement of all 27 hydrogen atoms, and although the derived metrical parameters must be viewed with the usual precautions, significant qualitative remarks can be made. The crystallographically imposed C_i symmetry requires the two lutetium atoms and the two hydrogen atoms to be coplanar. These data, combined with the similarity of the two Lu-H bond lengths, 2.16 (4) and 2.13 (4) Å, show the central core to be of approximately rhombic geometry with each hydride ligand bridging the two metal centers in a symmetrical fashion. The Lu-H distances in $[Cp_2LuH(THF)]_2$, 1.98 (6) and 2.13 (6) Å,[43c] appear to be comparable in magnitude. The present H-Lu-H* and Lu-H-Lu* angles are acute (75 (2)°) and obtuse (105 (2)°), respectively. The disparity in these angles is less than in either the neutron diffraction-derived structure of $[Cp'_2ThH(\mu\text{-}H)]_2$ (58 (1)° and 122 (4)°)[50] or the X-ray structures of $[(CH_3C_5H_4)_2ZrH(\mu\text{-}H)]_2$ (60 (1)°, 120 (1)°)[51] and $[Cp_2LuH(THF)]_2$ (62 (2)° and 118 (3)°).[43c]

$R_2SiCpCp''MCHTMS_2$ Hydrogenolysis Intermediates. Structure and Reactivity. Monitoring the relatively slow $R_2SiCpCp''MCHTMS_2$ hydrogenolysis process (eq 6) by ^1H NMR reveals the presence of intermediates in low, approximately steady-state concentrations through the course of the reaction (Figure 5). The relative spectral intensities for the $Et_2SiCpCp''LuCHTMS_2$ intermediate **16** (eq 6) are consistent with a 1:1 combination of $Et_2SiCpCp''LuCHTMS_2$ and $Et_2SiCpCp''LuH$ fragments (the Lu-H signal at δ 4.50 was confirmed using D_2 for the synthesis), while the presence of eight

(46) Höck, N.; Oroschin, W.; Paolucci, G.; Fischer, R. D. *Angew. Chem., Int. Ed. Engl.* **1986**, *25*, 738-739.

(47) Wells, A. F. *Structural Inorganic Chemistry*, 5th ed.; Oxford University Press: Oxford, 1989; pp 1286-1288.

(48) Pauling, L.; Kamb, B. *Proc. Natl. Acad. Sci. U.S.A.* **1986**, *83*, 3569-3571.

(49) Evans, W. J.; Meadows, J. H.; Wayda, A. L.; Hunter, W. E.; Atwood, J. L. *J. Am. Chem. Soc.* **1982**, *104*, 2015-2017.

(50) Broach, R. W.; Schultz, A. J.; Williams, J. M.; Brown, G. M.; Manriquez, J. M.; Fagan, P. J.; Marks, T. J. *Science* **1979**, *203*, 172-174.

(51) Jones, S. B.; Petersen, J. L. *Inorg. Chem.* **1981**, *20*, 2889-2894.

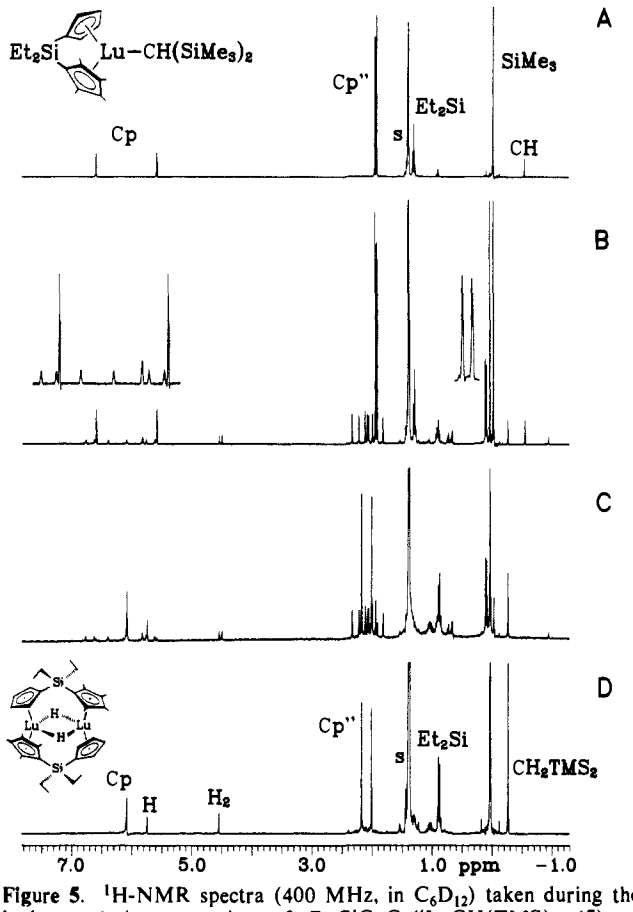

Figure 5. ^{1}H-NMR spectra (400 MHz, in C_6D_{12}) taken during the hydrogenolytic conversion of $Et_2SiCpCp''LuCH(TMS)_2$ (**5**) to $(Et_2SiCpCp''LuH)_2$ (**13**). (A) and (D) are spectra of **5** and **13**, respectively, while (B) and (C) are spectra taken before the hydrogenolysis is complete. The s represents a trace of $C_6D_{11}H$.

$Cp''-CH_3$, eight Cp–H, one CH, and two $Si-CH_3$ signals argues for a single isomer of relatively low symmetry (e.g., low-symmetry conformations of L, M, or N with restricted rotation about the relevant metal-ligand bonds). Parallel experiments with $Et_2SiCpCp''YCHTMS_2$ suggest the presence, in this case, of *two*

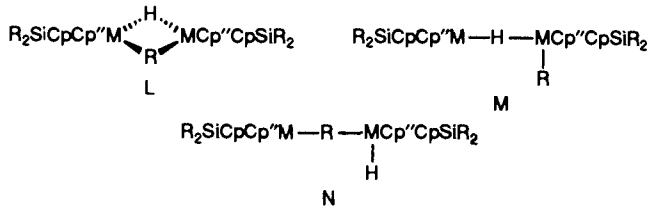

intermediates. Thus, two sets of eight $Cp''-CH_3$ and eight Cp–H resonances along with two C–H resonances are observed in a ratio of ca. 1.3:1. In regard to connectivity, the C(α)–H ^{1}H and ^{13}C resonances are each split by ^{89}Y into *doublets* (^{1}H δ −0.83, $^2J_{^{89}Y-H}$ = 2.6 Hz; δ −0.45, $^2J_{^{89}Y-H}$ = 2.8 Hz; ^{13}C δ 27.4, $^1J_{^{89}Y-^{13}C}$ = 32.8 Hz, $^1J_{^{13}C-H}$ = 91.2 Hz, δ 25.6, $^1J_{^{89}Y-^{13}C}$ = 31.8 Hz, $^1J_{^{13}C-H}$ = 93.3 Hz) arguing against bridging structures such as L or M as well as against rapid intramolecular exchange of the R group between M centers in M. The magnitudes of $J_{^{13}C-H}$ in these groups argue for the hybridization of a terminal metal hydrocarbyl (vide supra).[3] Unfortunately, the Y-H proton resonances were not detected in these intermediates and are presumed to be obscured by the $Cp''-CH_3$ signals.

The hydrogenolysis intermediates may be generated on a synthetic scale and isolated, albeit contaminated with both the starting alkyl and product dihydride. This isolation is easier for **4** than for **5** due to the limited solubility of the former. Although conditions were not optimized, slow stirring of a pentane solution of **4** under H_2 at 0 °C for 6 h, followed by cold filtration, affords the intermediate $(Me_2SiCpCp''Lu)_2(\mu\text{-}H)(CHTMS_2)$ (**15**) in ca.

Scheme I. Examples of Cp'_2M- and $Me_2SiCp''_2M$-Centered Olefin Chemistry (M = Lanthanide)

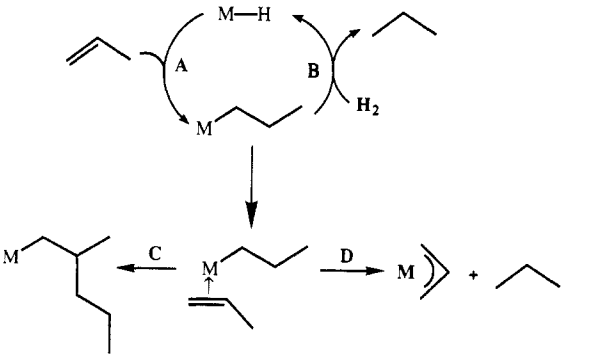

30% purity (as judged by ^{1}H NMR). Attempts to generate pure **16** by other routes were unsuccessful. Thus, attempted ligand redistribution (eq 7) yields no detectable **16** over a period of hours at 25–100 °C in toluene, while stoichiometric hydrogenation (eq 8) affords a mixture of dihydride **13**, intermediate **15**, and unreacted **5**.

$$\underset{\mathbf{13}}{\tfrac{1}{2}(Et_2SiCpCp''LuH)_2} + \underset{\mathbf{5}}{Et_2SiCpCp''LuCH(TMS)_2} \rightarrow \mathbf{16} \quad (7)$$

$$2\underset{\mathbf{5}}{Et_2SiCpCp''LuCH(TMS)_2} + H_2 \rightarrow \mathbf{5} + \mathbf{13} + \mathbf{16} \quad (8)$$

The proposed structures for **15** and **16** (L–N) suggest potential precursors of highly unsaturated/reactive species and thus prompted survey studies of catalytic properties. It was found that compound **16** is an active catalyst (or precatalyst) for ethylene polymerization with a turnover frequency of ~34 h^{-1} at 25 °C/1 atm of C_2H_4. There appears to be little induction period since white flakes of polyethylene are visible in the reaction solution within minutes. When generated in situ, **16** is also an active 1-hexene hydrogenation catalyst. Thus, rapidly stirring a solution of **5** and 1-hexene in toluene at 25 °C, under 1 atm of H_2, results in hydrogen uptake and an initial hydrogenation turnover frequency (at 2 h reaction time) of ~21 h^{-1}. However, catalytic hydrogenation slows dramatically as **5** and **16** are converted to the catalytically inactive (vide infra) product dihydride **13**. After another 3 h, the turnover frequency falls to $\lesssim$4 h^{-1}, and no hydrogen uptake is detectable after 11 h.

Since both $R_2SiCpCp''MCHTMS_2$ and $(R_2SiCpCp''MH)_2$ complexes are also present in samples of the hydridoalkyl intermediate, control catalytic experiments were conducted with these compounds. As will be discussed in the following section, the binuclear dihydrides are catalytically inefficient for ethylene polymerization and olefin hydrogenation. However, and in contrast to $Cp''_2MCHTMS_2$ and $Me_2SiCp''_2MCHTMS_2$ complexes,[3,31] $R_2SiCpCp''MCHTMS_2$ complexes are active for ethylene polymerization. That N_t for **5**, ~0.9 h^{-1} at 25 °C/1 atm pressure, is less than for **16** argues that **16** is the more active catalyst, perhaps as an $R_2SiCpCp''MH$ precursor. NMR monitoring of the **5** + ethylene reaction indicates that $\lesssim$1% of **5** is consumed during the formation of significant quantities of polyethylene. This result implies that the polymerization propagation rate (insertion into $M(-CH_2CH_2-)R$ bonds) is far more rapid than the initiation rate (insertion into the comparatively strong[52] M–C bond of a bulky $CHTMS_2$ moiety) or that a prior reaction is rate-limiting (e.g., vinylic C–H activation[53] to yield a more reactive M–$CH{=}CH_2$ bond + H_2CTMS_2).

Chemistry of Ring-Bridged Dinuclear Lanthanide Hydrides. Structure and Dynamics of Olefin Insertion Products. The unusual

(52) (a) Nolan, S. P.; Stern, D.; Marks, T. J. *J. Am. Chem. Soc.* **1989**, *111*, 7844–7853. (b) Nolan, S. P.; Stern, D.; Hedden, D.; Marks, T. J. *ACS Symp. Ser.* **1990**, *428*, 159–174. (c) Evans, W. J.; Ulibarri, T. A.; Ziller, J. W. *J. Am. Chem. Soc.* **1990**, *112*, 2314–2324.

(53) (a) Thompson, M. E.; Baxter, S. M.; Bulls, A. R.; Burger, B. J.; Nolan, M. C.; Santarsiero, B. D.; Schaefer, W. P.; Bercaw, J. E. *J. Am. Chem. Soc.* **1987**, *109*, 203–213. (b) Parkin, G.; Bunel, E.; Burger, B. J.; Trimmer, M. S.; van Asselt, A.; Bercaw, J. E. *J. Mol. Catal.* **1987**, *41*, 21–39.

lanthanide environment in **12–14** raises the intriguing question of whether different modes or degrees of reactivity are possible vis-à-vis the highly reactive Cp'_2M– and $Me_2SiCp''_2M$-based systems. As summarized in Scheme I, these latter complexes undergo rapid,[3] exothermic[52,54] olefin insertion into M–H bonds (pathway A). Rapid, reversible predissociation of the dimeric hydrides (eq 9) has been identified either kinetically[3b] or spectroscopically.[55] The resulting metal alkyl bonds undergo facile hydrogenolysis (pathway B),[3,56] olefin insertion[3,31,57] (pathway C),

$$\tfrac{1}{2}(Cp'_2MH)_2 \rightleftarrows Cp'_2MH \qquad (9)$$

and allylic C–H activation[31,52] (pathway D). In addition, the hydrides undergo C–H activation with exogenous hydrocarbons (including MH → MD conversions using deuterated hydrocarbons)[2g,3,31,53,58] and rapid exchange with D_2.[3,53,59]

Attempts were first made to detect/induce dissociation of binuclear hydrides **12–14**. Variable-temperature ^{1}H-NMR studies of **14** revealed persistence of sharp $^1J_{^{89}Y-H}$ triplets up to +90 °C, indicating the absence of rapid dissociation/intermolecular Y–H exchange. Furthermore, heating compound **13** in THF for 3 days at 60 °C gave no NMR spectroscopic evidence for dissociation/formation of $R_2SiCpCp''M(H)$·base species.[2g,53,58] In regard to C–H activation, neither **13** nor **14** evidences significant MH/MD exchange with benzene-d_6, toluene-d_8, pyridine-d_5, or cyclohexane-d_{12} over periods of many days at room temperature nor upon prolonged heating in toluene-d_8 at 145 °C. In comparison, $(Cp'_2LuH)_2$ and $(Me_2SiCp''_2LuH)_2$ undergo rapid exchange with deuterated arenes at room temperature.[2g,3,31] Solutions of **13-*d*** do undergo exchange with H_2; however, completion of this process requires several hours at 60 °C. In contrast, analogous exchange is rapid for $(Cp'_2MH)_2$ complexes[3,31] and is even rapid on the NMR time scale for Cp'_2ScH[53] and $(Cp'_2ThH_2)_2$.[59a]

In contrast to the $Cp'_2/Me_2SiCp''_2$-based hydrides and alkyls, the reaction of hydrides **12–14** with ethylene at atmospheric pressure does not yield polyethylene. Instead, 1 equiv of ethylene undergoes reversible insertion into a μ-H bond to afford hydridoethyl complexes in quantitative yield (by ^{1}H NMR) at room temperature (eq 10).[59b] See the Experimental Section for

$$(Et_2SiCpCp''MH)_2 + \| \underset{k_{-1}}{\overset{k_1}{\rightleftharpoons}} (Et_2SiCpCp''M)_2(\mu\text{-H})(\mu\text{-}CH_2CH_3) \qquad (10)$$

13, 14

17; M = Lu
17-*d*, M = Lu; H = D
18, M = Y

preparative scale reactions and analytical data. The molecular geometries of **17** and **18** (O) follow from low-temperature NMR spectra (e.g., Figure 6[27]) and are confirmed by diffraction (vide infra). Thus, the presence of four Cp″–Me and four Cp–H signals (the latter with appropriate coupling patterns) implies preservation of the magnetic equivalence of the Cp″ and Cp pairs of **12–14** (Figure 4) but loss of the $M(\mu\text{-H})_2M$ mirror symmetry, i.e., idealized C_{2h} → idealized C_2 symmetry.

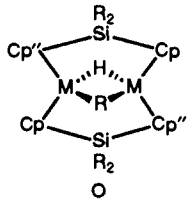

O

Table IX. ^{1}H-NMR Spectral Parameters for the α-Methylene Proton Exchange Process in Binuclear Lanthanide μ-Hydridoalkyls

compound	17	18	19	21
T_c (K)	294	312	284	288
δ $H_{\alpha 1}$	−1.76	−2.18	−1.10	−1.52
δ $H_{\alpha 2}$	0.15	0.17	0.15	0.71
$\Delta\nu$ (Hz)[b]	762	939	498	891
$\Delta\delta$ (ppm)[b]	1.91	2.35	1.25	2.21
$\Delta G^{\ddagger}$ (at T_c, kcal/mol)[c]	12.9	13.5	12.6	12.5

[a] Parameters for the exchange process of the two diastereotopic hydrogen atoms on the α-carbon atom. All measurements were carried out at 400 MHz in toluene-d_8. [b] Chemical shifts and shift differences at −80 °C. [c] Rate constants and $\Delta G^{\ddagger}$ (T_c) data calculated from coalescence data for a simple two-site exchange process. Calculations in the intermediate exchange regime based on bandwidth calculations yield similar activation parameters. Uncertainties are estimated to be ±0.5 kcal/mol.

The presence of a (bridging) hydride in **17** is confirmed spectroscopically by a resonance at δ 5.01 that is absent in **17-*d***. Furthermore, the IR spectra of **17** and **17-*d*** reveal strong bridging (Table V) metal hydride stretching transitions at 1273 (920, ν_{Lu-H}/ν_{Lu-D} = 1.38) cm^{-1}. In the ^{1}H-NMR spectrum of **18**, the Y–H signal appears as a triplet (δ 2.34; $^1J_{^{89}Y-H}$ = 38.6 Hz), again consistent with a bridging hydride. The ethyl portion of the ^{1}H spectrum of **17** appears as an ABX_3 pattern at low temperatures (vide infra; Figure 6 (supplementary material)) with the diastereotopic methylene protons strongly sensing the disymmetric C_2 environment. That the pairs of Cp″ and Cp ligands are each magnetically equivalent suggests that rotation of the μ-Et group about the μ-H–μ-C axis is rapid on the NMR time scale at this temperature (e.g., eq 11). These equivalences persist down to −85 °C. Selective decoupling and spin simulation (Figure 7 (supplementary material)[27]) experiments yield the parameters δ_A = −1.55, δ_B = 0.03, δ_X = 0.13, and $^3J_{H_A,H_X} = {}^3J_{H_B,H_X}$ = 7.9 Hz, and

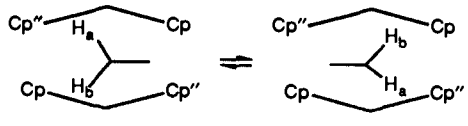

(11)

$^2J_{H_A,H_B}$ = −10.5 Hz. These are unexceptional for a variety of CH_3CH_2X moieties.[60] The ^{13}C-NMR spectrum of $(Et_2SiCpCp''Lu)_2(\mu\text{-H})(\mu\text{-}^{13}CH_2{}^{13}CH_3)$ (**17-*1,2*-$^{13}C_2$** prepared from **13** + $^{13}CH_2{}^{13}CH_2$) at −60 °C reveals $^1J_{^{13}C-H}$ = 107 and 125 Hz for the methylene and methyl carbon atoms, respectively. While the former parameter is small in magnitude, it is not exceptional for "bent" ($\angle$M–C–M ≪ 180°) f-element μ-alkyl arrangements[38,61] nor for some terminal alkyl groups.[38,62] The identical coupling constants for the two methylene protons is in agreement with the proton–proton coupling data which suggest similar hybridization for the two methylene C–H bonds.

As the temperature of a toluene-d_8 solution of **17** is raised from −60 °C, the diastereotopic methylene proton signals broaden, coalesce, and finally sharpen to a single (quartet) resonance (Figure 8). These changes are reversible with temperature and independent of concentration over a 9-fold range. No other signals in the ^{1}H or ^{13}C spectra are interchanged (e.g., four Cp″–Me and four Cp–H signals remain). Additional evidence that the con-

(54) (a) Bruno, J. W.; Marks, T. J.; Morss, L. R. *J. Am. Chem. Soc.* **1983**, *105*, 6825–6832. (b) Bruno, J. W.; Stecher, H. A.; Morss, L. R.; Sonnenberger, D. C.; Marks, T. J. *J. Am. Chem. Soc.* **1986**, *108*, 7275–7280. (c) Sonnenberger, D. C.; Morss, L. R.; Marks, T. J. *Organometallics* **1985**, *4*, 352–355. (d) Schock, L. E.; Marks, T. J. *J. Am. Chem. Soc.* **1988**, *110*, 7701–7715, and references therein.

(55) Watson, P. L.; Herskovitz, T. *ACS Symp. Ser.* **1983**, *212*, 459–479, and references therein.

(56) Lin, Z.; Marks, T. J. *J. Am. Chem. Soc.* **1987**, *109*, 7979–7985, and references therein.

(57) Lin, Z.; Marks, T. J. *J. Am. Chem. Soc.* **1990**, *112*, 5515–5525.

(58) Evans, W. J.; Chamberlain, L. R.; Ulibarri, T.; Ziller, J. W. *J. Am. Chem. Soc.* **1988**, *110*, 6423–6432.

(59) (a) Fagan, P. J.; Manriquez, J. M.; Maatta, E. A.; Seyam, A. M.; Marks, T. J. *J. Am. Chem. Soc.* **1981**, *103*, 6650–6667. (b) Owing to appreciably lower starting material and product solubilities, the analogous insertion chemistry of **12**, while clearly observable by NMR, was not pursued on a preparative scale.

(60) Silverstein, R. M.; Bassler, G. C.; Morrill, T. C. *Spectrometric Identification of Organic Compounds*, 4th ed.; Wiley: New York, 1981; Chapter 5.

(61) Ozawa, F.; Park, J. W.; Mackenzie, P. B.; Schaefer, W. P.; Henling, L. M.; Grubbs, R. H. *J. Am. Chem. Soc.* **1989**, *111*, 1319–1327, and references therein.

(62) Mann, B. E.; Taylor, B. F. *^{13}C NMR Data for Organometallic Compounds*; Academic Press: New York, 1981; pp 38–85.

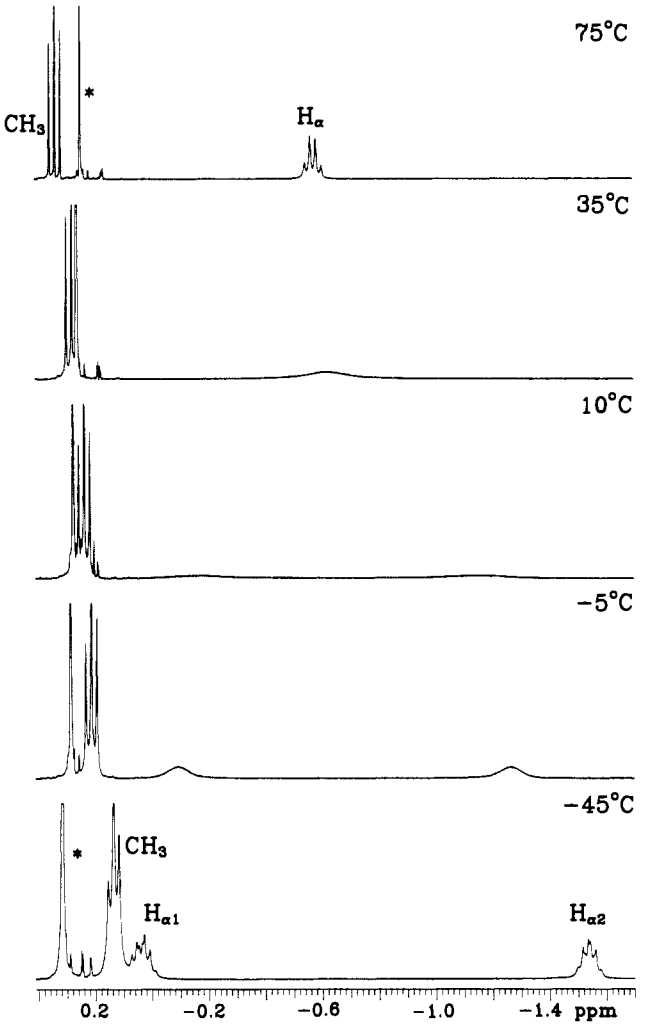

Figure 8. Upfield portion of the ^{1}H-NMR spectrum of $(Et_2SiCpCp''Lu)_2(\mu\text{-}H)(\mu\text{-}C_2H_5)$ (**17**) dissolved in toluene-d_8, at various temperatures. The * denotes a trace impurity.

nectivity of the M(μ-H, μ-Et)M bridging geometry remains fixed in this process derives from **17** and **17**-*1,2*-$^{13}C_2$, where the μ-H and μ-^{13}C signals remain sharp triplets over the entire temperature range. Similar behavior is observed in other μ-hydrido-μ-alkyls (vide infra). Relevant spectral parameters and free energies of activation estimated via the coalescence point simplification of the modified Bloch formalism[63] are set out in Table IX. The mechanism of this unusual dynamic process will be taken up in the Discussion section.

Two types of experiments were conducted in an effort to identify "agostic" α or β M···H interactions in the hydridoalkyl structures. Infrared spectral data for **17**, **17-*d***, and **18** are compiled in the Experimental Section. Diagnostic of "agostic" M···H···C interactions in many transition-metal complexes are low-frequency ν(C-H) (2700–2300 cm^{-1}) stretching modes.[28] In the present case, the IR spectra of **17**, **17-*d***, and **18** do not reveal obvious features in the 2800–1500-cm^{-1} region. Note that such evidence does not a priori rule out agostic interactions, as the IR spectra of both **4** (and its analogues) and $Cp'_2Th(CH_2CMe_3)_2$[27a] do not evidence such features, although NMR and diffraction evidence suggests α-agostic interactions[6a] in both. Partial deuteration experiments in which differential C-H/C-D zero-point energy effects in C-H···M vs C-H configurations give rise to proton shift differences ($\Delta\delta$) offer another means to probe for these interactions.[63] For this purpose, $(Et_2SiCpCp''Lu)_2(\mu\text{-}H)(\mu\text{-}CHDCH_2D)$ (**17-*1,2-d*$_2$**) was prepared by reaction of **13** with *trans*-ethylene-*1,2-d*$_2$. At low temperature (-45 °C), the chemical shift differences between **17-*1,2-d*$_2$** and **17** for $H_{\alpha 1}$, $H_{\alpha 2}$, and H_β are $\Delta\delta$ = 0.147, 0.142, and 0.058 ppm, respectively, while just below coalescence (-3 °C, vide infra), these differences are 0.140, 0.130, and 0.046, respectively. At 60 °C (in the fast exchange regime) the coalesced H_α peak evidences an isotope shift of $\Delta\delta$ = 0.125, while the analogous C_β proton shift is 0.048. Since the low-temperature data are similar for both methylene hydrogen atoms, this result again argues that the C(α)-H groups are in similar bonding environments. The present $\Delta\delta$ parameters can be compared to corresponding values observed for CH_3X (0.010), $Cp_2W(CH_2X)_2$ (0.020), Cp'_2ScCH_2X (0.057), and $Cp'_2Sc^{13}CH_2{}^{13}CH_2X$ (0.090), where X = H or D.[53] In these systems, NMR evidence for α- or β-agostic interactions is inconclusive, although vibrational spectroscopic data suggest an $\overline{ScCH_2CH_3}$ interaction in the latter compound.[53] In contrast to these early transition element/f-element results, bridge-terminal M···H/M···D equilibria are readily evident in NMR spectra of $XOs_3(CO)_{10}CH_2X$ (X = H or D) where $\Delta\delta$ is larger in magnitude and more temperature-dependent: 0.34 at 35 °C and 0.55 at -76 °C.[64] In summary, the present μ-hydrido-μ-alkyls offer no compelling spectroscopic evidence for strong α- or β-M···HC "agostic" interactions.

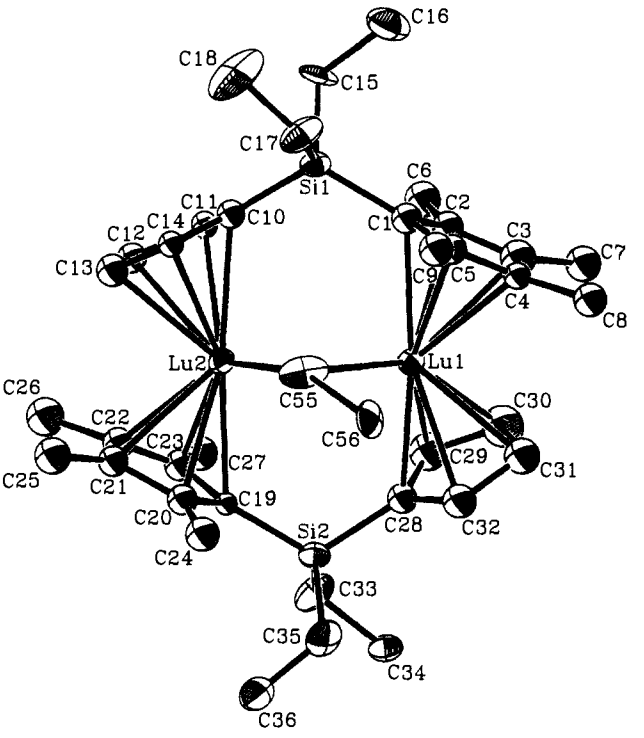

Figure 9. Perspective ORTEP view of the molecular structure of $(Et_2SiCpCp''Lu)_2(\mu\text{-}H)(\mu\text{-}C_2H_5)$ (**17**). All atoms are represented by thermal ellipsoids drawn to encompass 50% probability.

Molecular Structure of $\{[C_2H_5]_2Si[C_5H_4][(CH_3)_4C_5]Lu\}_2(\mu\text{-}H)(\mu\text{-}C_2H_5)$ (17). The crystallographic results for **17** are in accord with the spectroscopic properties, as can be seen in the ORTEP diagram (Figure 9). Atomic coordinates can be found in Table X (supplementary material) and anisotropic thermal parameters in Table XI (supplementary material).[27] Selected bond lengths and angles are summarized in Table XII. Although the precision of the present diffraction study is less than for **4** and **13** (see Experimental Section for details), significant conclusions can be drawn.

The spanning disposition of the supporting $Et_2SiCpCp''$ ligation and the associated metrical parameters in **17** are nearly identical with those observed in dihydride **13** (Table VIII, vide supra). As in **13** and in contrast to **4**, there does not appear to be significant strain at the bridging silicon atoms (Si1 and Si2), as evidenced by nearly tetrahedral valence angles. Average Lu-C(ring) distances in **17** are 2.60 (2, 1, 5, 3, 10)[34] and 2.59 (1.8, 4, 8, 10) Å for the C_5H_4 and Me_4C_5 ligands, respectively. The Lu1-Lu2 distance, 3.392 (1) Å, is again relatively short and is identical within experimental uncertainty with that in **13** (3.390 (1) Å). As mentioned in the structural discussion for **13**, this short vector does not necessarily imply extensive Lu-Lu bonding and is more likely a consequence of the bridging ligation environment.

Table XII. Selected Bond Lengths (Å) and Angles (deg) in the Coordination Groups of $(Et_2SiCpCp''Lu)_2(\mu\text{-}H)(\mu\text{-}C_2H_5)$ (**17**)[a]

Lu1–C1	2.55 (2)	Lu2–C12	2.61 (2)
Lu1–C2	2.58 (2)	Lu2–C13	2.60 (2)
Lu1–C3	2.66 (2)	Lu2–C14	2.57 (2)
Lu1–C4	2.62 (2)	Lu2–C19	2.51 (1)
Lu1–C5	2.62 (2)	Lu2–C20	2.61 (2)
Lu1–C28	2.62 (2)	Lu2–C21	2.66 (2)
Lu1–C29	2.59 (2)	Lu2–C22	2.56 (2)
Lu1–C30	2.58 (2)	Lu2–C23	2.57 (2)
Lu1–C31	2.61 (2)	Lu2–C55	2.46 (2)
Lu1–C32	2.61 (2)	Si1–C1	1.89 (2)
Lu1–C55	2.58 (2)	Si1–C10	1.82 (2)
Lu1–C56	2.78 (2)	Si2–C19	1.85 (2)
Lu2–C10	2.63 (2)	Si2–C28	1.88 (2)
Lu2–C11	2.61 (1)	C55–C56	1.64 (2)
Lu1–C55–C56	79 (1)	C17–Si1–C15	107 (1)
Lu2–C55–C56	148 (1)	C33–Si2–C35	108 (1)
Lu1–C55–Lu2	84.7 (5)	Cg–Lu–Cg[b]	127.8
C1–Si1–C10	116 (1)	Cg–Lu–Cg[c]	128.1
C19–Si2–C28	115 (1)		

[a] Only metrical parameters for the ordered molecule in the unit cell are given. Metal-ring and intraring parameters for the disordered molecule are in excellent agreement with these. A full tabulation of distances and angles is given in the supplementary material. [b] C1–C4 ring centroid–Lu1–C28–C32 ring centroid. [c] C10–C14 ring centroid–Lu2–C19–C23 ring centroid.

The most interesting structural feature of **17** is the unusual coordination geometry of the μ-ethyl ligand. While a significant number of homometallic transition and f-element μ-alkyl complexes have been diffractometrically characterized,[61,65] **17** is, to our knowledge, the first μ-ethyl complex of this type to be characterized. As is evident in Figure 9, the μ-ethyl geometry in **17** is highly unsymmetrical in several respects. Thus, Lu2–C55 = 2.46 (2) Å while Lu1–C55 = 2.58 (2) Å. These distances are somewhat longer than terminal Lu–C(alkyl) bonds, as exemplified by Lu–C(α) = 2.365 (7) Å in **4** and 2.344 (12) Å in $Cp'_2Lu(\mu\text{-}CH_3)LuCp'_2(CH_3)$.[2g] They are, however, more comparable to the Lu–(μ-CH_3) distances in the latter compound, 2.440 (9) and 2.756 (9) Å. Correcting for differences in lanthanide eight-coordinate ionic radii, the present Lu–C(α) distances are also comparable to those in more symmetrically bridged $[Cp_2Y(\mu\text{-}CH_3)]_2$ and $[Cp_2Yb(\mu\text{-}CH_3)]_2$ (G):[35] Y–C = 2.553 (10), 2.537 (9) Å (2.51, 2.50 Å when corrected); Yb–C = 2.536 (17), 2.486 (17) Å (2.53, 2.48 Å when corrected). Furthermore, the present ∠Lu1–C55–Lu2 value of 84.7 (5)° is comparable to ∠Y–C–Y = 87.7° and ∠Yb–C–Yb = 86.6° in the latter two compounds.

In addition to the inequality of Lu–C55 bond lengths in **17**, the orientation of the μ-ethyl group is highly unsymmetrical (Figure 9). Thus, there is a large disparity in the two Lu–C55–C56 angles, 148 (1)° and 79 (1)°. The combination of this rather acute angle with the short Lu1–C56 distance of 2.78 (2) Å (cf., the Lu–"agostic"CH_3 distance of 2.820 (8) Å in **4** and the longer Lu–μ-CH_3 bond of 2.756 (9) Å in $Cp'_2Lu(\mu\text{-}CH_3)LuCp'(CH_3)$) suggests a significant secondary interaction between Lu1 and the β methyl group (e.g., P). It would appear that the present ethyl

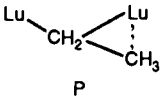

P

group C55–C56 distance of 1.64 (2) Å reflects some lengthening of this parameter; however, this is near the edge of statistical (3σ)

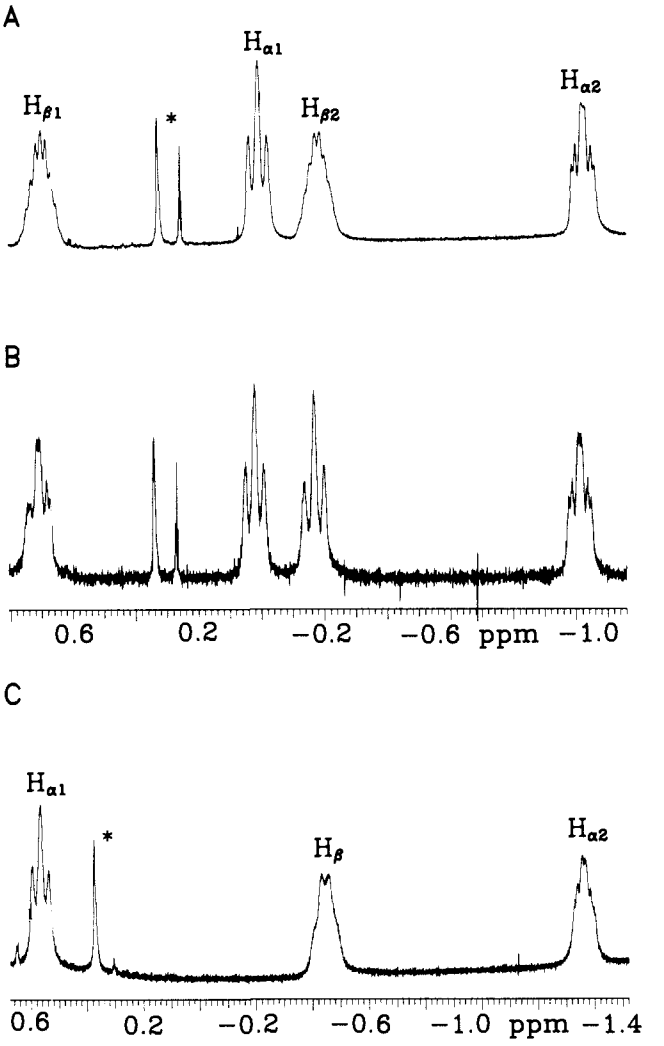

Figure 10. Upfield portion of the low-temperature (−60 °C) ^{1}H-NMR spectrum of (A) $(Et_2SiCpCp''Lu)_2(\mu\text{-}H)(\mu\text{-n-}C_3H_7)$ (**19**) dissolved in toluene-d_8. (B) Same as (A) but with irradiation at the location of the *n*-propyl methyl resonance (δ 1.10). (C) Upfield portion of the low-temperature ^{1}H-NMR spectrum (−70 °C) of $(Et_2SiCpCp''Lu)_2(\mu\text{-}H)(\mu\text{-n-}C_6H_{13})$ (**21**) dissolved in toluene-d_8. The * denotes a trace impurity.

significance.[66] Interestingly, the $^1J_{^{13}C-^{13}C}$ values observed in **17**-$^{13}C_2$ and **18**-$^{13}C_2$ (25 and 24 Hz, respectively) are significantly lower than typically observed for sp^3C–Csp^3 structures (35–40 Hz)[67] and are explicable in terms of decreased C–C bond order.[68] The metrical data also evidence an ~0.4-Å displacement of C56 from the Lu1–C55–Lu2 plane in the direction of Si2.

μ-Hydrido Olefin Insertion Chemistry. Scope, Regiochemistry, and Product Characteristics. In contrast to Cp'_2- and $Me_2SiCp''_2$-based organolanthanide hydrides, the reaction of $(Et_2SiCpCp''LuH)_2$ (**13**) with propylene or 1-hexene is not extremely rapid and yields neither olefin oligomers nor η^3-allyl structures (Scheme I). Rather, bridging hydride/μ-alkyl complexes are formed quantitatively (as assayed by ^{1}H NMR) at room temperature (eqs 12 and 13). Compounds **19** and **21** were also synthesized on a preparative scale and characterized by standard methodology (see Experimental Section). The assignment of structure Q for **19**–**21** follows from NMR spectral data, which

(63) Sandstrom, J. *Dynamic NMR Spectroscopy*; Academic Press: New York, 1982; pp 77–99, and references therein.
(64) (a) Calvert, R. B.; Shapley, J. R.; Schultz, A. J.; Williams, J. M.; Suib, S. L.; Stucky, G. D. *J. Am. Chem. Soc.* **1978**, *100*, 6240–6241. (b) Calvert, R. B.; Shapley, J. R. *J. Am. Chem. Soc.* **1978**, *100*, 7726–7727. (c) Calvert, R. B.; Shapley, J. R. *J. Am. Chem. Soc.* **1977**, *99*, 5225–5226.
(65) (a) Holton, J.; Lappert, M. F.; Pearce, R.; Yarrow, P. I. W. *Chem. Rev.* **1983**, *83*, 135–201, and references therein. (b) Waymouth, R. M.; Santarsiero, B. D.; Coots, R. J.; Bronikowski, M. J.; Grubbs, R. H. *J. Am. Chem. Soc.* **1986**, *108*, 1427–1441, and referenes therein.
(66) C–C distances of 1.5466 (4) and 1.5470 (4) Å in the μ_3-CH_2CH_3 groups of $(LiEt)_4$ give no indication of such lengthening: Dietrich, H. *J. Organomet. Chem.* **1981**, *205*, 291–299.
(67) (a) Marshall, J. L. *Carbon–Carbon and Carbon–Proton NMR Couplings*; Verlag Chemie International: Deerfield Beach, FL, 1983; Chapter 3. (b) Wehrli, F. H.; Marchand, A. P.; Wehrli, S. *Interpretation of Carbon-13 NMR Spectra*, 2nd ed.; John Wiley: New York, 1983; pp 81–84. (c) Weigert, F. J.; Roberts, J. D. *J. Am. Chem. Soc.* **1972**, *94*, 6021–6025.
(68) The present result is also in accord with well-documented $^1J_{C_xCH_3} \sim {}^1J_{C_xH}$ proportionalities.[67]

$(Et_2SiCpCp''MH)_2$ + ⟋⟍ ⇌ $(Et_2SiCpCp''M)_2(\mu\text{-H})(\mu\text{-}n\text{-}C_3H_7)$ (12)

13, 14 **19**, M = Lu; **20**, M = Y

$(Et_2SiCpCp''LuH)_2$ + ⟋⟍C_4H_9 $\underset{k_{-1}}{\overset{k_1}{\rightleftharpoons}}$ $(Et_2SiCpCp''Lu)_2(\mu\text{-H})(\mu\text{-}n\text{-}C_6H_{13})$ (13)

13 **21**

are reminiscent of **17** and **18** (see Experimental Section). Thus,

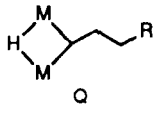

Q

R = H (**19**, **20**), *n*-C_4H_9 (**21**)

resonances attributable to magnetically equivalent sets of Cp and Cp'' ligands as well as a μ-H group (a triplet in **20** with $^1J_{^{89}Y\text{-}H}$ = 38.4 Hz) are easily identified. The μ-*n*-propyl fragment of **19** is readily analyzed in the −60 °C spectrum by the observed multiplicities and spin decoupling experiments (Figure 10A,B). It can be seen that both the C_α and C_β methylene proton pairs exhibit large diastereotopic shifts. This effect is even larger in compound **21** (Figure 10C).[69]

Upon warming solutions of either **19** or **21**, corresponding pairs of diastereotopic C_α methylene signals broaden, collapse, and merge to single resonances. Magnetization-transfer experiments further confirm the identities of the permuted sites. As noted above for **17** and **18**, the Cp, Cp'', μ-H, and R_2Si resonances of **19** and **21** are *unaffected* by this fluxional process, as are the other diastereotopic μ-alkyl methylene resonances. Spectral and activation parameters are set out in Table IX. From the similarity of spectral changes and $\Delta G^\ddagger$ values, it is inferred that the exchange mechanism is the same for all members of the μ-hydrido-μ-alkyl series.

Questions about the regiochemistry of eqs 10, 12, and 13 include whether secondary μ-alkyls can be formed as kinetic or thermodynamic products and the site of initial μ-H delivery in the insertion process. Monitoring of eqs 12 and 13 by NMR gave no indication of organolanthanide species other than dihydride and product hydridoalkyl. Heating **14** + additional propylene for up to 3 days at 100 °C in toluene-d_8 gave no evidence of μ-isopropyl products (nor of a dialkyl or multiple insertion product). Interestingly, attempts to effect the thermal isomerization of **19** in the absence of excess propylene revealed that an equilibrium mixture of hydridoalkyl and dihydride, and olefin is formed on prolonged heating. Similar behavior is observed for **21**, and further information on these equilibration processes will be given in the following section. Insertion experiments were also conducted with internal olefins in an effort to produce secondary μ-alkyls or to detect hydrozirconation-like addition/isomerization activity. However, no reaction was observed when solutions of **13** and olefins such as *cis*-2-butene and *trans*-2-hexene were heated for periods of up to 4 days at 80 °C. Clearly hydrozirconation-like reactivity patterns are not facile. When excess ethylene is allowed to react with **13-*d*** at room temperature, ^1H and ^{13}C NMR reveal the exclusive formation (>98%) of $(Et_2SiCpCp''Lu)_2(\mu\text{-D})(\mu\text{-}CH_2CH_2D)$ (**17-*d*-2-*d*$_1$**, eq 14). Subsequent scrambling of the label in the product is only anticipated at higher temperatures (vide infra).

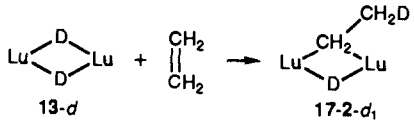

13-*d* **17-2-d_1** (14)

Efforts were also made to measure the rate of hydrogenolysis of the μ-*n*-propyl bond in **20**. Although detailed kinetic studies were not carried out, NMR experiments place the second order rate constant (assuming a simple bimolecular mechansim[56]) at ~1 × 10^{-4} M^{-1} s^{-1} (25 °C).

(69) The resonance for the other C_β proton of **20** is located in the region of overlapped signals attributable to C_γ–C_δ and $SiEt_2$ protons. Integration of this region versus the observed $H_{\alpha 1}$, H_β, and $H_{\alpha 2}$ signals supports this contention.

Table XIII. Second-Order Rate Constant Data for the Insertion of 1-Hexene into One of the Lu(μ-H)Lu Bonds of $(Et_2SiCpCp''LuH)_2$ (**13**)

complex	olefin	T (°C)	k (M^{-1} s^{-1})
$(Et_2SiCpCp''LuH)_2$, **13**	1-hexene	45.5	1.34 (2) × 10^{-4}
		55.4	2.65 (6) × 10^{-4}
		65.5	4.6 (1) × 10^{-4}
		74.9	7.3 (1) × 10^{-4}
$(Et_2SiCpCp''LuD)_2$, **13-*d***	1-hexene	65.5	3.3 (1) × 10^{-4}

Table XIV. Activation Parameters, Kinetic Isotope Effects, and Thermodynamic Parameters Describing the Reversible Insertion of 1-Hexene into One of the μ-Hydride Bonds of $(Et_2SiCpCp''LuH)_2$ (**13**) in Toluene-d_8

	insertion	elimination[d]
E_a, kcal/mol	12.8 (4)[a]	24.1 (6)
log A	4.9 (3)[a]	9.8 (3)
$\Delta H^\ddagger$, kcal/mol	12.0 (4)[b]	22.8 (6)
$\Delta S^\ddagger$, eu	−38.6 (7)[b]	−13 (2)
$\Delta G^\ddagger$, kcal/mol	24.7 (8)[c]	27.4 (7)
k_H/k_D	1.4 (1)[e]	
ΔH	−10.7 (6)	
ΔS	−25 (2)	

[a] From Arrhenius plot. [b] From Eyring plot. [c] Calculated for T = 60 °C. [d] Calculated from the difference between the activation data for the insertion process and the thermodynamic parameters (see Figure 13). [e] Kinetic isotope effect measured at 65 °C.

Kinetic and Equilibrium Studies of Olefin Insertion into M(μ-H)M Bonds. As already noted, 1-hexene undergoes reversible insertion into the M(μ-H)M bond of **13** to form the μ-hydrido-μ-alkyl complex **21** (eq 13). The progress of this reaction, at temperatures where the position of eq 13 lies far to the right (45–75 °C for the concentrations of **13** and olefin used), was followed by monitoring ^1H NMR resonances for either the appearance of product **21** or the disappearance of the starting hydride (see Experimental Section for details). Reaction rates determined by either method were indistinguishable, and no species other than starting materials and product were observed. Under pseudo-zero-order conditions in olefin (≥15 equiv of 1-hexene), the reaction was found to be first-order in metal complex. A representative kinetic plot is shown in Figure 11A, and the dependence of the observed, pseudo-first-order rate constant on olefin concentration (Figure 11B) indicates the rate law of eq 15. The

$$v = k[\mathbf{13}][\text{1-hexene}] \quad (15)$$

temperature dependence of the insertion rate was measured (45–75 °C), and derived second-order rate constants are listed in Table XIII. Satisfactory Arrhenius (Figure 12) and Eyring plots were obtained, and derived activation parameters are set out in Table XIV. A study of 1-hexene insertion into the analogous deuteride **13-*d*** was also carried out, and a kinetic isotope effect of k_H/k_D = 1.4 (1) at 65 °C was determined.

It was found that the equilibria in eqs 10, 12, and 13 are temperature-dependent and can be cycled repeatedly without detectable decomposition. Thus, heating solutions of **17**–**21** above 140 °C drives the respective equilibria completely to dihydride + olefin, while subsequent cooling below ca. 80 °C slowly regenerates the corresponding hydridoalkyls. The system **13** ⇄ **21** + 1-hexene was studied in toluene-d_8 solution over the range 95–125 °C, allowing ample time to establish equilibrium at each temperature (see Experimental Section). Thermodynamic parameters[70] from a van't Hoff analysis of the data are set out in Table XIV.

Efforts were also made to detect complexation between ethylene and **13** prior to insertion (e.g., eq 16). Several diamagnetic, early

(70) (a) The standard state concentration is 1.0 mol L^{-1}.[70b,c] (b) Robinson, P. J. *J. Chem. Ed.* **1978**, *55*, 509–510. (c) Benson, S. W. *Thermochemical Kinetics*, 2nd ed.; Wiley: New York, 1986; pp 8–10.

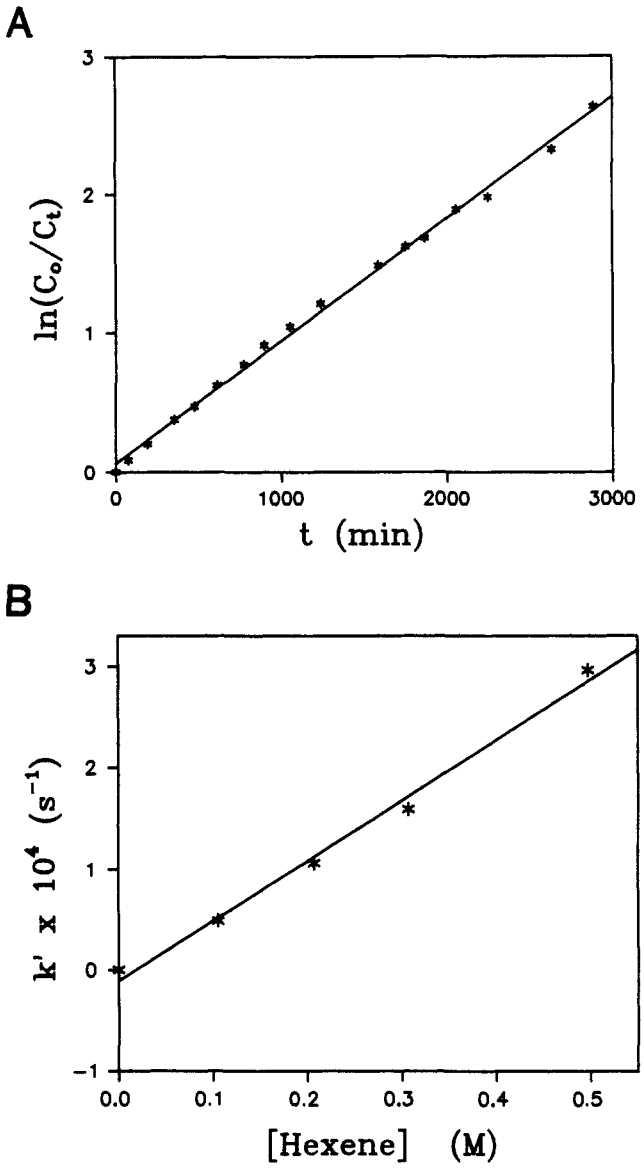

Figure 11. (A) Kinetic plot for the insertion of 1-hexene into one of the Lu(μ-H)Lu bonds of $(Et_2SiCpCp''LuH)_2$ (**13**) at 45 °C. (B) Plot of the pseudo-first-order rate constant k' versus 1-hexene concentration for the insertion of 1-hexene into one of the Lu(μ-H)Lu bonds of $(Et_2SiCpCp''LuH)_2$ (**13**) at 65 °C.

transition-metal olefin complexes are known and exhibit ethylene upfield ^1H NMR coordination shifts of 3–4 ppm.[71] Studies were conducted with a toluene-d_8 solution of **13** and ethylene (1 atm) over the temperature range +25 to −60 °C. No shift in the dissolved ethylene peak was observed, nor were any new spectral


(16)

features detected. Assuming that the system is at fast exchange and that the chemical shift difference between bound and free ethylene is >1 ppm, it can be estimated that less than 0.5% of the lanthanide complex is present as an olefin complex under these conditions.[72] A 1:1 organoeuropium–ethylene complex has recently been detected by using paramagnetic NMR techniques.[73] It is labile and the ethylene binding constant small.[74]

Discussion

This study provides a number of key points of structure, reactivity, and thermodynamic information relevant to understanding as well as designing early transition element and f-element homogeneous catalysts and reagents. In the following discussion, we focus in a comparative fashion upon the ramifications of $R_2SiCpCp''$ ancillary ligation, structure, molecular dynamic, thermodynamic, reactivity properties of μ-alkyl ligands and how these properties contrast with those of Cp'_2MR and $Me_2SiCp''_2MR$ analogues.[3,31]

$R_2SiCpCp''$ Ancillary Ligation. In comparison to earlier findings for Cp'_2M and $Me_2SiCp''_2M$ complexes,[3,27b,30,31] the present $Me_2SiCpCp''LuCHTMS_2$ (**4**) structural results reveal significant reduction in ancillary ligand steric encumbrances about the lanthanide coordination sphere as evidenced by the Lu–$CHTMS_2$ bond length and Cp,Cp″–CHTMS nonbonded distances. In terms of how these structural factors might affect reactivity, the kinetic ordering $R_2SiCpCp''MR > Me_2SiCp''_2MR > Cp'_2MR$ is found for sterically demanding olefin insertion processes such as ethylene polymerization[3b,31] and hydroamination/cyclization.[7] In the latter transformation, intramolecular olefin insertion into an M–N bond is turnover-limiting, and relative turnover frequencies for the above three Lu ancillary ligation arrays are 200:75:≪1, respectively.[7] Interestingly, this trend does not obtain for sterically less sensitive M–alkyl bond hydrogenolysis,[56] where $R_2SiCpCp''LuCHTMS_2$ is significantly *less* reactive than the $Me_2SiCp''_2Lu$ and Cp'_2Lu analogues.[3,31] The reason may be due to the sterically allowed, closer Lu–$CHTMS_2$ interaction (evident in the diffraction results for **4** but not in thermochemical measurements[52b,75]) or to less effective charge stabilization in the four-center heterolytic transition state (R, L_n = $R_2SiCpCp''$ would be a weaker donor).

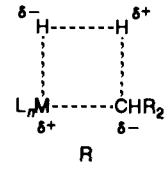
R

In regard to modulating reactivity at lanthanide centers, $R_2SiCpCp''$ ancillary ligation clearly accelerates olefin insertion processes vis-à-vis the $Me_2SiCp''_2$ and Cp'_2 analogues. However, it also facilitates an irreversible, deactivating $2R_2SiCpCp''M \rightarrow M(\mu\text{-}R_2SiCpCp'')_2M$ rearrangement process under hydrogenolysis conditions. The hydrogenolysis of $R_2SiCpCp''MCHTMS_2$ complexes most likely proceeds via a highly unsaturated $R_2SiCpCp''MH$ species which rapidly undergoes reaction with starting alkyl to form a complex of stoichiometry $(R_2SiCpCp''M)_2(H)(CHTMS_2)$. This intermediate probably has a structure such as L or N. The reactivity of the intermediate with respect to hydrogenolysis or ethylene insertion argues that rearrangement to a far more inert μ-hydridoalkyl $M(\mu\text{-}R_2SiCpCp'')_2M$ structure (O) has not yet occurred at this stage in the reaction sequence. The facility of the rearrangement in comparison to the $Me_2SiCp''_2$ analogues apparently reflects the smaller steric demands of $R_2SiCpCp''$ coordination, which may stabilize dinuclear precursors to the $M(\mu\text{-}R_2SiCpCp'')_2M$ rearrangement product (e.g., L or N). In addition, the more weakly donating Cp portion of the ligand may not be as strongly bound, and hence may be more labile with respect to intermetal exchange processes than the $Me_2SiCp''_2$ analogue.

Pathways to and Distinctive Properties of μ-Alkyl Ligands. The present μ-alkyl complexes were prepared by olefin addition to the

(71) (a) Burger, B. J.; Santarsiero, B. D.; Trimmer, M. S.; Bercaw, J. E. *J. Am. Chem. Soc.* **1988**, *110*, 3134–3146, and references therein. (b) Doherty, N. M.; Bercaw, J. E. *J. Am. Chem. Soc.* **1985**, *107*, 2670–2682, and references therein.

(72) Further support for this contention is derived from spin–lattice relaxation time studies which indicate that the T_1 of dissolved ethylene is, within experimental error, unchanged by the addition of **13**.

(73) Nolan, S. P.; Marks, T. J. *J. Am. Chem. Soc.* **1989**, *111*, 8538–8540.

(74) For other types of organolanthanide complexes with simple olefins and acetylenes, see: (a) Burns, C. J.; Andersen, R. A. *J. Am. Chem. Soc.* **1987**, *109*, 915–917 $(Cp'_2Yb(\mu\text{-}C_2H_4)Pt(PEt_3)_2)$. (b) Burns, C. J.; Andersen, R. A. *J. Am. Chem. Soc.* **1987**, *109*, 941–942 $(Cp'_2Yb(MeC_2Me))$.

(75) Relative to an assumed constant D(Lu–I), we find[52b] $D(Cp'_2Lu\text{–}CHTMS_2)$ = 67.0 (1.8) kcal/mol, $D(Me_2SiCp''_2Lu\text{–}CHTMS_2)$ = 62.4 (1.8) kcal/mol, and $D(Et_2SiCpCp''Lu\text{–}CHTMS_2)$ = 55.1 (1.8) kcal/mol.

corresponding μ-H complexes (eq 10). A priori, the kinetic data do not rule out a free radical pathway[76] for this process (e.g., eqs 17 and 18); however, the considerable strength of Lu–H bonds (D(Lu–H) $\approx$ 67 kcal/mol[52b]) and the observed product regio-

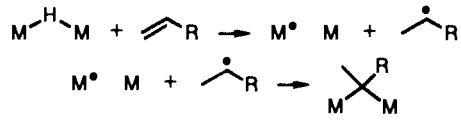

(17)

(18)

chemistry (eqs 12 and 13) argue against it.[77] More plausible is a four-center insertion process (eq 19).[57,71] While the kinetic data

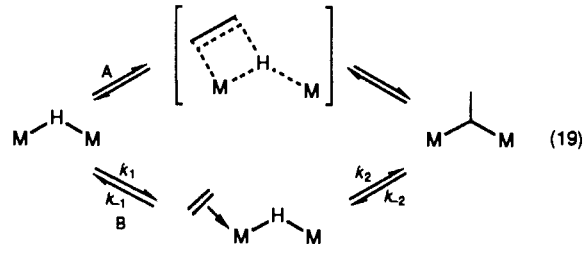

(19)

do not distinguish between a concerted addition (A) and certain stepwise scenarios involving a π complex intermediate (B), the aforementioned efforts to detect such intermediates (vide supra) indicate that $k_1/k_{-1} \ll 1$ and that k_{-1} is large. Thermodynamic data (vide infra) indicate that k_2/k_{-2} is also large. Furthermore, the observed Lu_2H/Lu_2D kinetic isotope effect of 1.4 (1) (at 65 °C) supports rate-limiting Lu_2–H cleavage and compares with effects of 1.3 (2)–1.4 (1) for olefin insertion into $Cp'_2Th(OR)H$ complexes,[57] 1.7 (6)–2.7 (1) for intramolecular insertion in $Cp'_2Nb(C_2H_4)H$,[71b] 1.15 for cyclohexene insertion in $RhH_2Cl_2(PPh_3)_2$,[78] and 1.87 (terminal addition), 1.78 (internal addition) for styrene hydroboration.[79] Assuming negligible tunneling and a fictitious Lu_2H diatomic, an approximate theoretical primary kinetic isotope effect of ca. 2.2 is estimated[80] from the vibrational spectroscopic data in Table V.

Regarding the quantitative question of whether the Lu(μ-H)$_2$Lu configuration offers enhanced reactivity over terminal Lu–H bonds with respect to olefin insertion, the present rate constant for 1-hexene insertion, 1.34 (2) $\times$ 10^{-4} M^{-1} s^{-1} (45.5 °C), can be compared with values obtained from organolanthanide-catalyzed olefin hydrogenation studies[3b] or from related work.[57] For $(Cp'_2LuH)_2$-catalyzed 1-hexene hydrogenation, which is presumed to involve monomeric species, the corresponding insertion rate constant must be >10^2–10^3 M^{-1} s^{-1} (25 °C) to be compatible with the observed, turnover-limiting rate of Lu(n-hexyl) hydrogenolysis.[3b] For bulkier cyclohexene, olefin addition to Cp'_2LuH is rate-limiting, and the corresponding rate constant is 2.3 $\times$ 10^{-2} M^{-1} s^{-1} (25 °C).[3b] For 1-hexene addition to more saturated/less reactive $Cp'_2An(OR)H$ complexes (An = actinide), second-order rate constants vary from >10^{-2} M^{-1} s^{-1} (30 °C) for An = U, R = t-Bu to 2.9 $\times$ 10^{-5} M^{-1} s^{-1} (60 °C) for highly congested An = Th, R = CH (t-Bu)$_2$.[57] These results offer no evidence that the μ-H geometry activates the Lu–H bond for olefin insertion and, in the most realistic comparisons, indicate a deactivating effect. Indeed, if the aforementioned reactivities in hydroamination/cyclization[7] are employed to derive a hypothetical Cp'_2LuH:$R_2SiCpCp''LuH$ reactivity ratio, it is concluded that the kinetic deactivation incurred upon placing the hydride ligand in a bridging position as in **13** is $\gtrsim 10^8$–10^{10}.

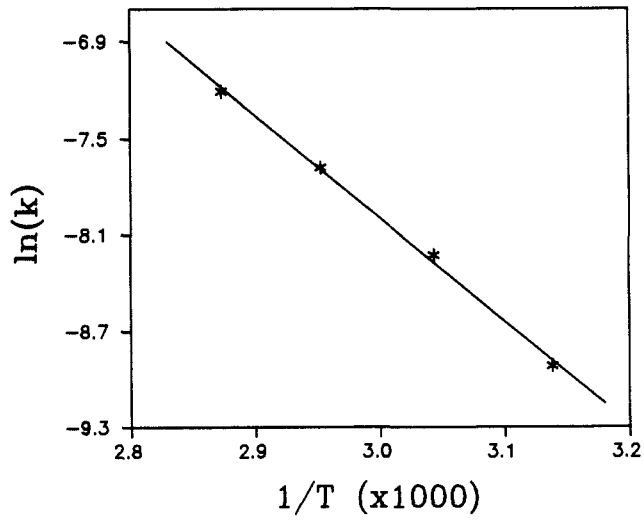

Figure 12. Arrhenius plot for the insertion of 1-hexene into one of the Lu(μ-H)Lu bonds of $(Et_2SiCpCp''LuH)_2$ (**13**). Units: k, M^{-1} s^{-1}; T, K.

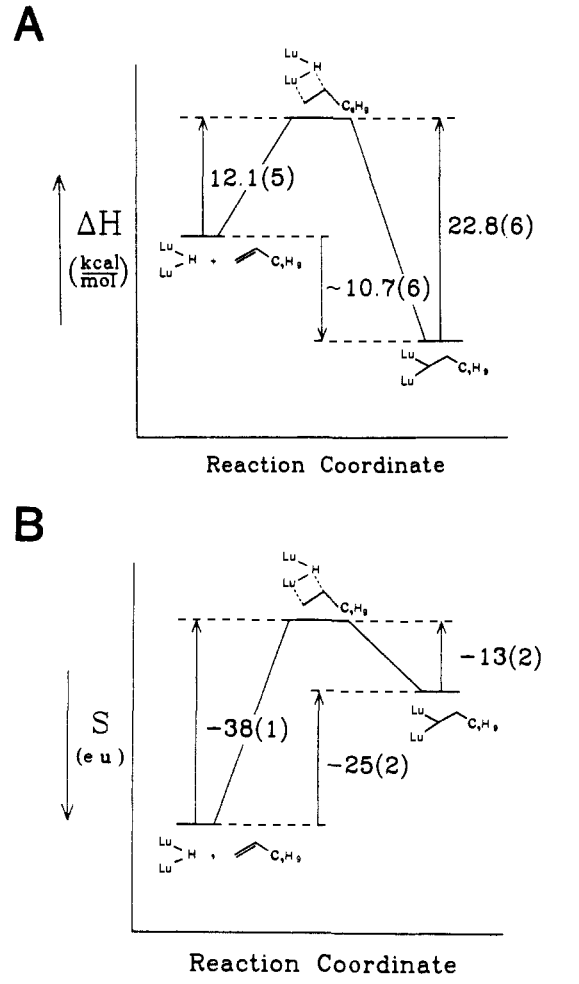

Figure 13. (A) Schematic enthalpic reaction coordinate for the insertion (eq 15) of 1-hexene into a Lu(μ-H)Lu bond of $(Et_2SiCpCp''LuH)_2$ (**13**). (B) Schematic entropic reaction coordinate for the insertion (eq 15) of 1-hexene into a Lu(μ-H)Lu bond of $(Et_2SiCpCp''LuH)_2$ (**13**).

Activation parameters and thermodynamic data for the **13** + 1-hexene $\rightleftharpoons$ **21** equilibrium are set out in Table XIV and enthalpic as well as entropic reaction coordinates are plotted in Figure 13. It can be seen that the enthalpy of activation is rather small while the entropy of activation is large and negative (not unusually so for a bimolecular process). These data suggest an organized transition state having significant bond making to compensate for the bond breaking. In comparison, the intermolecular Cp'_2Th-(O-t-Bu)H + cyclohexene insertion process occurs with $\Delta H^{\ddagger}$ =

(76) Sweany, R. L.; Halpern, J. *J. Am. Chem. Soc.* **1977**, *99*, 8335–8337.
(77) If efficient capture of the resulting ethyl radical is assumed (eq 18 and 19, R = H), then the labeling results of eq 14 are, in principle, compatible with a radical mechanism.
(78) Halpern, J.; Okamoto, T.; Zakhariev, A. *J. Mol. Catal.* **1976**, *2*, 65–68.
(79) Pasto, D. J.; Kang, S. Z. *J. Am. Chem. Soc.* **1968**, *90*, 3790–3800.
(80) Using the approximate relationship $k_1/k_2 = e^{[0.7193(r_1-r_2)/T]}$. Buddenbaum, W. E.; Shiner, V. J., Jr. In *Isotope Effects on Enzyme-Catalyzed Reactions*; Cleland, W. W., O'Leary, M. H., Northrop, D. B., Eds.; University Park Press: Baltimore, MD, 1977; Chapter 1.

9.0 (5) kcal/mol and $\Delta S^{\ddagger} = -47.2$ (1) eu,[57] while for *intramolecular* insertion in $Cp'_2Nb(C_2H_4)H$, $\Delta H^{\ddagger} = 14.7$ (1) kcal/mol and $\Delta S^{\ddagger} = -11.2$ (2.9) eu, and in *cis*-$HRh(C_2H_4)[P(i\text{-}Pr)_3]_2$, $\Delta H^{\ddagger}$ = 13.0 kcal/mol and $\Delta S^{\ddagger} = -2$ eu.[79] Figure 13 reveals that $\Delta H^{\ddagger}$ for β-H elimination in **21** is considerably larger than for the addition process and, interestingly, that $\Delta S^{\ddagger}$ for elimination is also negative. This suggests that the transition state for β-H elimination in **21** also requires a significant degree of organization. Comparative quantitative kinetic information on β-H elimination processes in f-element alkyls is sparse because the process is frequently endothermic (vide infra) and/or because competing processes (H abstraction from proximate ligands,[1b,2d] β-Me elimination[45]) intervene. For $Cp'_2Lu(CH_2CHMe_2)$, $\Delta G^{\ddagger}$ (25 °C) for β-H elimination is ~23 kcal/mol,[45] while extensive label scrambling in the Cp'_2MD-catalyzed D_2 + cyclohexene reaction under mass transport-limited D_2 suggests rapid addition/elimination sequences.[3b] For $Cp'_2An(OR)$(*sec*-butyl) → $Cp'_2An(OR)$(*n*-butyl) isomerization, which presumably involves β-H elimination/readdition, $\Delta G^{\ddagger}$ (25 °C) ~23–24 kcal/mol.[57] In contrast, coordinatively saturated Cp_3AnR complexes resist thermal β-H elimination up to high temperatures.[81]

The present data also provide the first quantitative information on f-element μ-H/μ-alkyl thermochemical relationships. In **21**, β-H elimination is endothermic by 10.7 (6) kcal/mol, implying that $D(Lu_2\text{-H}) - D(Lu_2\text{-alkyl}) \approx 24$ kcal/mol.[82] The only terminal D(M-alkyl) data presently available for comparison is for $CHTMS_2$ complexes,[52] which may not be strictly comparable. Assuming for the moment that attractive "agostic" and repulsive steric effects approximately cancel and that $CHTMS_2$ is a reasonable first approximation to a primary alkyl, then $D[(Cp'_2Lu\text{-H})_2] - D(Cp'_2Lu\text{-}CHTMS_2) \approx 0$ kcal/mol and $D[(Me_2SiCp''_2Sm\text{-H})_2] - D(Me_2SiCp''_2Sm\text{-}CHTMS_2) \approx 10$ kcal/mol.[52] These comparisons indicate that organolanthanide μ-alkyl bonding enjoys no unusual stabilization vis-ā-vis μ-H bonding and may in fact be destabilized versus terminal alkyls. Data for actinide alkoxyl alkyls also exhibit small D(M-H) - D(M-alkyl) values ($D(Cp'_2Th(OR)\text{-H}) - D(Cp'_2Th(OR)\text{-}n\text{-butyl}) \approx 6$ kcal/mol,[54b]), while larger values are observed in $D[Cp'_2Th(H)\text{-H})]_{average} - D[Cp'_2Th(n\text{-butyl})\text{-}n\text{-butyl}], \approx 24$ kcal/mol[54d] and $D[Cp'(Cp''CH_2CH_2CH_3)Hf(H)\text{-H}] - D[Cp'(Cp''CH_2CH_2CH_2)Hf\text{-H}] \approx 23$ kcal/mol.[83] In the platinum series, $D(L_2Pt(Cl)\text{-H}) - D(L_2Pt(Cl)\text{-Et}) \approx 23$ kcal/mol (L = PEt_3).[84] The present data therefore provide no compelling evidence that lanthanide μ-alkyl linkages are exceptionally strong and suggest, instead, that they may be relatively weak vis-ā-vis the corresponding μ-hydrides. Thermodynamic instability with respect to β-H elimination certainly rationalizes the paucity of transition element μ-alkyls having β-H substituents,[65] and any extra instability, as suggested above, would enhance this effect.

The present thermochemical data yield $\Delta S = 25$ (2) eu for β-H elimination. This quantity may be somewhat smaller than anticipated on the basis of 1 particle → 2 particles increases in translational entropy;[85] however, it is in excellent agreement with $\Delta S = 27.0$ (1.3) eu reported for β-H elimination in $L_2Pt(Cl)Et$ (vide infra).[84]

Although detailed kinetic studies were not carried out, qualitative comments can be made about the hydrogenolytic reactivity of the μ-alkyl functionality in **19**. NMR experiments indicate that the rate constant at room temperature is $\sim 1 \times 10^{-4}$ M^{-1} s^{-1}. In contrast, the corresponding parameters obtained from studies of catalytic 1-hexene hydrogenation are 7.7×10^4 and 2.6×10^4 M^{-1} s^{-1} for $Cp'_2Lu(n\text{-hexyl})$ and $Me_2SiCp''_2Lu(n\text{-hexyl})$, respectively,[3b] again indicating the severe deactivating characteristics of the bridging coordination environment. Importantly, the present thermochemical results indicate that the lower hydrogenolytic reactivity of μ-alkyl groups is not a consequence of a greater metal–alkyl bond strength.

In regard to molecular dynamic aspects of μ-alkyl coordination, the disymmetry of the O-type molecular framework permits observation of a new rearrangement process in addition to previously observed[65] rotation about the μ-H–M–C(α) vector. This intramolecular rearrangement permutes diastereotopic μ-alkyl C_α methylene protons without creating a time-averaged mirror plane perpendicular to the idealized molecular C_2 axis (e.g., without accessing the site occupied by μ-H), without involving the μ-H ligand and without effecting rapid exchange of C_α and C_β protons (as might occur in rapid β-H elimination–readdition sequences[86]). Rather, inversion at the C_α carbon best explains the spectroscopic permutation pattern. This is schematized in eq 21 where $\angle H_1\text{–}C_\alpha\text{–}H_2 \approx 180°$ is a pseudorotation-like[87] transition state and $\angle < 180°$ suggests S_E1-like character. This inversion process is reminiscent of those observed in lithium alkyls.[88] Here theoretical studies implicate a "planar" methyl group transition state similar to that in eq 20.[89]

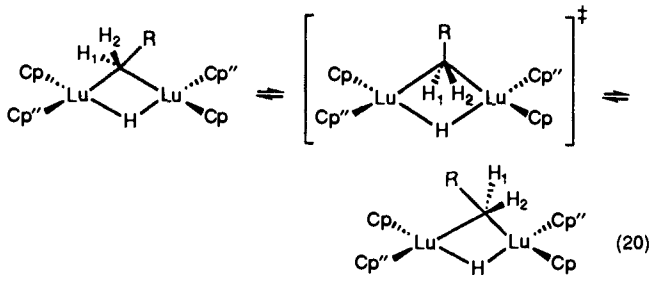

Conclusions

The present results indicate that seemingly incremental adjustments in organo-f-element coordinative unsaturation can lead to previously unrecognized ligand redistribution processes having drastic consequences for certain modes of reactivity. In addition, this study provides the first quantitative, comparative kinetic, and thermochemical information on the properties of organo-f-element μ-hydride and μ-alkyl ligands. The substantial decrease in reactivity observed is presumably both steric and electronic in origin, with the latter certainly reflecting electronic population of otherwise empty metal-centered LUMO levels.[6,44,90] For these highly electrophilic metal centers, the availability of such orbitals is no doubt crucial in modulating reactivity.[44a] Any diminished thermodynamic stability of μ-alkyl bonding, especially in comparison to terminal alkyls and μ-hydrides, must certainly involve steric factors as well as the favorable directional characteristics/overlap of the H 1s orbital versus an alkyl sp^3 orbital in M(μ-X)M bridging geometries.

(81) (a) Bruno, J. W.; Kalina, D. G.; Mintz, E. A.; Marks, T. J. *J. Am. Chem. Soc.* **1982**, *104*, 1860–1869. (b) Marks, T. J.; Wachter, W. A. *J. Am. Chem. Soc.* **1976**, *98*, 703–710, and references therein. (c) Marks, T. J.; Seyam, A. M.; Kolb, J. R. *J. Am. Chem. Soc.* **1973**, *95*, 5529–5539.

(82) (a) In these estimates, we employ standard thermochemical parameters for the organic fragments[82b–d] and assume metal effects largely attenuate within two σ bonds. (b) McMillan, D. F.; Golden, D. M. *Ann. Rev. Phys. Chem.* **1982**, *33*, 493–532. (c) Reference 70c, Appendix. (d) Griller, D.; Kanabus-Kaminska, J. M.; Maccoll, A. *J. Mol. Struct.* **1988**, *163*, 125–131.

(83) Bulls, A. R.; Bercaw, J. E.; Manriquez, J. M.; Thompson, M. E. Metal–Ligand Bonding Energetics in Organotransition Metal Compounds. In *Polyhedron Symposium-in-Print*; Marks, T. J., Ed.; 1988; Vol. 7, pp 1409–1428.

(84) Brainard, R. L.; Whitesides, G. M. *Organometallics* **1985**, *4*, 1550–1557.

(85) (a) Smith, G. M.; Carpenter, J. D.; Marks, T. J. *J. Am. Chem. Soc.* **1986**, *108*, 6805–6807. (b) Page, M. I. In *The Chemistry of Enzyme Action*; Page, M. I., Ed.; Elsevier: New York, 1984; pp 1–54. (c) Page, M. I.; Jencks, W. F. *Proc. Natl. Acad. Sci. U.S.A.* **1971**, *68*, 1678–1683.

(86) Brookhart, M.; Lincoln, D. M.; Volpe, A. F., Jr.; Schmidt, G. F. *Organometallics* **1989**, *8*, 1212–1218, and references therein.

(87) Berry, R. S. *J. Chem. Phys.* **1960**, *32*, 933–938.

(88) (a) Wardell, J. L. in ref 1b, Chapter 2. (b) Fraenkel, G.; Beckenbaugh, W. E.; Yang, P. P. *J. Am. Chem. Soc.* **1976**, *98*, 6878–6885. (c) Witanowski, M.; Roberts, J. D. *J. Am. Chem. Soc.* **1966**, *88*, 737–741. (d) Whitesides, G. M.; Witanowski, M.; Roberts, J. D. *J. Am. Chem. Soc.* **1965**, *87*, 2854–2862.

(89) (a) Clark, T.; Schleyer, P. v. R.; Pople, J. A. *J. Chem. Soc., Chem. Commun.* **1978**, 137–138. See, also: (b) Schleyer, P. v. R.; Tidor, B.; Jemmis, E. D.; Chandrasekhar, J.; Würthein, E. U.; Kos, A. J.; Luke, B. T.; Pople, J. A. *J. Am. Chem. Soc.* **1983**, *105*, 484–488. (c) Jemmis, E. D.; Chandrasekhar, J.; Schleyer, P. v. R. *J. Am. Chem. Soc.* **1979**, *101*, 527–533.

(90) Krüger, C.; Sekutowski, J. C.; Berke, H.; Hoffmann, R. *Z. Naturforsch. B* **1978**, *33*, 1110–1115.

Acknowledgment. We are grateful to NSF for support of this research under Grant CHE8800813. We also thank Mr. Xin Min Yang for assistance with several experiments.

Supplementary Material Available: Tables of positional and anisotropic thermal parameters for **4** (Tables II and III), **13** (Tables VI and VII), and **17** (Tables X and XI), a full tabulation of important bond distances and angles for **4**, **13**, and **17**, and Figures 1, 6, and 7 (39 pages); listings of observed and calculated structure factors from the final cycle of least-squares refinement (92 pages). Ordering information is given on any current masthead page.

Intrazeolite Metal Carbonyl Topotaxy. A Comprehensive Structural and Spectroscopic Study of Intrazeolite Group VI Metal Hexacarbonyls and Subcarbonyls

Saim Özkar,[†,‡] Geoffrey A. Ozin,[*,‡] Karin Moller,[§] and Thomas Bein[§]

Contribution from the Lash Miller Chemistry Department, University of Toronto, Toronto, Ontario, Canada M5S 1A1, and Department of Chemistry, University of New Mexico, Albuquerque, New Mexico 87131. *Received January 3, 1990*

Abstract: This paper focuses attention on the intrazeolite anchoring, thermal decarbonylation, ligand exchange, and addition chemistry of $M(CO)_6$-$M'_{56}Y$, where M = Cr, Mo, W; M' = H, Li, Na, K, Rb, Cs. The key points to emerge from this study include the following. (i) $M(CO)_6$-$M'_{56}Y$ samples have the hexacarbonylmetal(0) molecule associated with two α-cage extraframework cations (or Brønsted protons), via the oxygen end of two trans bonded carbonyls with a saturation loading of $2M(CO)_6/\alpha$-cage. (ii) $M(CO)_6$-$M'_{56}Y$ samples have the hexacarbonylmetal(0) guest confined to the internal surface of the zeolite with a homogeneous distribution throughout the zeolite crystals. (iii) A Mo and Rb EXAFS structure analysis of $8\{Mo(CO)_6\}$-$Rb_{56}Y$ shows that the α-cage encapsulated $Mo(CO)_6$ guest maintains its structural integrity, with some evidence for anchoring via extraframework Rb^+ cations. (iv) A rapid ^{13}CO intrazeolite ligand exchange occurs for $M(^{12}CO)_6$-$M'_{56}Y$ to yield $M(^{12}CO)_m(^{13}CO)_{6-m}$-$M'_{56}Y$, the extent of which depends on the ^{13}CO loading. (v) $M(CO)_3$-$M'_{56}Y$ can be cleanly generated via the mild vacuum thermal decarbonylation of $M(CO)_6$-$M'_{56}Y$, the tricarbonyl stoichiometry of which is unequivocally established from its observed and calculated diagnostic $M(^{12}CO)_n(^{13}CO)_{3-n}$-$M'_{56}Y$ vibrational isotope pattern and from EXAFS structural data. (vi) Intrazeolite reactions of $M(CO)_3$-$M'_{56}Y$ with large and small arenes, trienes, and phosphines cleanly yield the respective intrazeolite six-coordinate complexes (shown to be identical with the products of direct impregnation of the latter complexes), thereby supporting the tricarbonylmetal(0) assignment as well as pinpointing the location of the $M(CO)_3$-$M'_{56}Y$ tricarbonylmetal(0) fragment on the internal surface of the zeolite. (vii) Cation effects in the mid/far-IR, EXAFS data, and optical reflectance spectra indicate that the supercage-confined $M(CO)_3$-$M'_{56}Y$ moiety is anchored to an oxygen framework site rather than to an extraframework cation site via the metal or oxygens of the carbonyls. (viii) The tricarbonyl fragments show C_s and C_{3v} symmetry depending on the choice of M and M' which can be rationalized in terms of a second-order Jahn-Teller effect. (ix) EXAFS data for the mild thermal decomposition of $Mo(CO)_3$-$Rb_{56}Y$ demonstrates the formation of molybdenum atoms statistically distributed in the zeolite lattice.

Introduction

Organometallics and coordination compounds strategically located and anchored within the cage and channel spaces of different zeolite structure types possess the ability to organize and effect catalytic and electrochemical transformations, artificial photosynthesis, gas separation/purification, and vectorial electron transport processes with molecule size/shape specificity.[1] While volatile organometallics are now routinely used as precursors for the fabrication of device quality semiconductor nanostructures using epitaxial MOCVD and photoepitaxy,[2] it is only very recently that they have been intentionally utilized to create organized assemblies of intrazeolite semiconductor quantum crystallites.[3] Intrazeolite organometallic (photo)topotaxy could provide a useful inroad to the chemical synthesis of semiconductor quantum dot, wire, and supralattice nanostructures with possible applications as quantum electronic and nonlinear optical devices.[4]

This paper focuses on simple binary metal carbonyls for the eventual growth and stabilization of intrazeolite semiconductor quantum structures.[5a] The rationale for selecting this particular group of precursors relates to their volatility, molecular dimensions, ease of purification, availability, and facile and quantitative conversion to the respective metal oxide materials with minimal contamination by carbon.[5a,b]

In this particular investigation we direct attention to the following: (i) anchoring site details of $M(CO)_6$ in $M'_{56}Y$ (where M = Cr, Mo, W; M' = H, Li, Na, K, Rb, Cs), (ii) internal versus external confinement and the homogeneity of $M(CO)_6$-$M'_{56}Y$, (iii) ^{13}CO isotope substitution chemistry of $M(CO)_6$-$M'_{56}Y$, (iv) vacuum thermal decarbonylation chemistry of $M(CO)_6$-$M'_{56}Y$ to $M(CO)_3$-$M'_{56}Y$, (v) $^{12}CO/^{13}CO$ mixed isotopic proof of the $M(^{12}CO)_n(^{13}CO)_{3-n}$-$M'_{56}Y$ stoichiometry, (vi) location and identity of $M(CO)_3$-$M'_{56}Y$ via arene, triene, and phosphine size exclusion chemical reactions, (vii) an EXAFS determination of

[†] On sabbatical leave from the Chemistry Department, Middle East Technical University, Ankara, Turkey.
[‡] University of Toronto.
[§] University of New Mexico.

(1) Ozin, G. A.; Gil, C. *Chem. Rev.* **1989**, *89*, 1749 and references cited therein.
(2) Almond, M. J.; Rice, D. A.; Yates, C. A. *Chem. Br.* **1988**, *24*, 1130.
(3) Ozin, G. A.; Kuperman, A.; Stein, A. *Adv. Mater.* **1989**, *101*, 373. Stucky, G. D.; MacDougall, J. *Science* **1990**, *247*, 669, and references cited therein.
(4) Brus, L. E., et al. *J. Mater. Res.* **1989**, *4*, 704.
(5) (a) Ozin, G. A.; Özkar, S. *J. Phys. Chem.* **1990**, *94*, 7556. Ozin, G. A.; Özkar, S.; Macdonald, P. *J. Phys. Chem.* **1990**, *94*, 6939. (b) Herrmann, W. A. *J. Organomet. Chem.* **1986**, *300*, 111. *Angew. Chem., Int. Ed. Engl.* **1988**, *27*, 1297. Almond, M. J.; Crayston, J. A.; Downs, A. J.; Poliakoff, M.; Turner, J. *Inorg. Chem.* **1986**, *25*, 19-25, and references cited therein.

0002-7863/90/1512-9575$02.50/0